

How did sediments disperse and accumulate in the oceanic basin, South China Sea



Fei Wang^a, Weiwei Ding^{b,a,*}

^a School of Oceanography, Shanghai Jiao Tong University, Shanghai, 200030, China

^b Key Laboratory of Submarine Geosciences & Second Institute of Oceanography, Ministry of Natural Resources, Hangzhou, 31002, China

ARTICLE INFO

Keywords:

Sediment budget
Sedimentary provenance
Controlling factors
IODP
Oceanic basin of South China Sea

ABSTRACT

Quantification of the sedimentary accumulation and dispersion process of the South China Sea (SCS) not only establishes an important part on the “source-to-sink” process in Southeast Asia, but also sheds lights on the submarine slope failure and associated submarine canyon/channels formation. Based on geological interpretations of more than 30 multichannel seismic profiles covering the whole oceanic basin with constraints from IODP Expedition drilling results, we calculated the sediment budget of the oceanic basin since the Oligocene on a million-year geological scale. Sediment isopach maps in different geological time were reconstructed to understand the controlling factors dominating the Cenozoic sedimentary accumulation and dispersion process, as well as the possible sedimentary provenances. Results show that the sediment budget of the whole oceanic basin increased gradually with time, although the rate has not been consistent over time. It was complicated by regional tectonics, including the spreading of the SCS, the uplift of the Tibet Plateau and Taiwan, changes in the Asian monsoon, rerouting and organization of the river systems, and sea level changes. Submarine channel/canyon systems developed in the continental margin acted as the major conduits for terrestrial sediments discharging into the oceanic basin. We observe two decrease trends in sediment accumulation rates occurred in the Southwest Sub-basin during the Late Miocene, and in the Northwest Sub-basin during the Pliocene. The former might be related with the local rifting event in the Mekong Shelf, which trapped most of the terrestrial input. While the later was due to the retreat of the Central Canyon and Pearl River Canyon in the Late Pliocene. Sediment isopach maps indicate that the sediment accumulation was dominantly in the northern flank of the SCS oceanic basin before the Late Miocene, with the depocenters generally distributed at the mouth of the channel/canyon systems and slope foot area near basement highs; the main depocenters gradually migrated to the southern flank of the basin since the Pliocene. This is likely due to an increase sediment from the Mekong River and the high sea level. An exception is the development of a new depocenter in the northeast related with the Taiwan orogeny. The primary sediment provenances include South China, Tibet Plateau, Indo-China Peninsula, and Taiwan Island, with minor contributions from the Hainan Island, Palawan, Luzon Islands, as well as local basement highs developed on the continental margin.

1. Introduction

The Tibetan Plateau uplift and formation of the West Pacific marginal seas are the two major tectonic events in Eurasian Mesozoic-Cenozoic geologic history. These two events induced the largest source-sink system in the world, that is, a huge amount of terrestrial sediment is transported from the Tibetan Plateau to the Indian Ocean and the West Pacific marginal seas. Understanding of this source to sink process needs an integral study on the continent uplifting, weathering and erosional events, evolution of the Asian monsoon, the development

of large Asian rivers, and the formation of marginal basins. As one of the largest marginal sea basins in West Pacific, the South China Sea (SCS) plays a significant role in mass transport and accumulation since the initial continental rifting in the Late Cretaceous. In general, the SCS is not only the crucial pathway for transporting terrigenous materials from Eurasia to the western Pacific Ocean since the Early Oligocene, but also the dominant accumulation and preservation place as a result of limited material exchange between the semi-closed oceanic basin and the open ocean since the Middle Miocene (Fig. 1A). Except for partial accumulation on land (such as riverbeds), most of the terrestrial sediments were

* Corresponding author. School of Oceanography, Shanghai Jiao Tong University, Shanghai, 200030, China.

E-mail address: wwding@sio.org.cn (W. Ding).

discharged and then accumulated in the SCS through different large fluvial drainage systems, such as the Pearl River, the Red River, and the Mekong River, etc. (Fig. 1B). This made the SCS reserved more than 700 million metric tons (Mt), accounting for 5.5% of the global total sediment mass with only 0.9% of the global sea area (Wang and Li, 2009; Milliman and Farnsworth, 2011; Liu et al., 2016). Hence, quantitative study of the sedimentary process and analytical prediction of the potential sedimentary provenance are keys to characterize the “Source-to-Sink” process in Southeast Asia, as well as to improve our understanding of the integrated effects on regional and local tectonic events, climate change, Asian monsoon, and eustatic fluctuation, etc. (Yang, 2006; Caracciolo, 2020). Sediment budget, as an important index of quantitative research describing sediments influx, storage, loss, and transport pathways in a geological system (Hapke et al., 2010), is currently a keynote aspect to study the accumulation and dispersion process of the SCS.

An ideal model of a sediment budget calculation is targeted on the whole sedimentary loading area, including the continental margin and the abyssal basin. Based on the abundant multichannel seismic data and more than 2000 industrial drilling data in its shelves and slopes, sediment budget of the continental margin of the SCS has been well studied (See Fig. 6 for details), such as the Pearl River Mouth Basin in the north (Clift, 2006; Clift et al., 2014), Yinggehai Basin and Qiongdongnan Basin in the northwest (Clift and Sun, 2006; Yan et al., 2011; Lei et al., 2015), the continental margin of Indo-China Peninsula in the west (Murray and Dorobek, 2004; Huang, 2004; Clift, 2006; Liu et al., 2007; Li et al., 2013), and the Nansha Area and North Palawan Area in the south (Huang, 2004). Clift and Sun (2006) calculated the sediment budgets of

the Qiongdongnan Basin and Yinggehai Basin, and reconstructed the regional sedimentary records to assess the relationship between Cenozoic Asian climatic structures and denudation. After that Yan et al. (2011) and Lei et al. (2015) verified this process by drawing isopach maps of sedimentary thickness and rate in the Yinggehai Basin based on dense interpreted seismic profiles. Clift (2006) also reconstructed the sediment budgets of the Pearl River Mouth Basin and Mekong Shelf using multichannel seismic data; while Li et al. (2012) and Xie et al. (2013) quantified the sedimentary recording of the Mekong Slope and Baiyun Sag respectively.

First attempt on the quantification of sediment budget in oceanic basin of the SCS was applied by Huang and Wang (2006). Their results showed that the SCS has a total sediment mass of 1.44×10^{10} Mt since the Oligocene. However, the lack of drilling sites in the oceanic basin greatly affected the accuracy of the calculation results.

In 2014 and 2017, the International Ocean Discovery Program (IODP) Expeditions 349, 367&368 drilled twelve sites in the oceanic basin of the SCS, six of which (U1431, U1433, U1434, U1500, U1502, and U1503) penetrated into the basaltic basement (Fig. 1C; Table 2; Li et al., 2015b; Sun et al., 2018), providing a complete sedimentary record of the Cenozoic strata. With these drilling results spanning from the initial oceanic crust to fossil spreading ridge, a well dated abyssal stratigraphy and identification of the lithology for each sedimentary unit are now possible. Yin et al. (2018) studied the sedimentary filling characteristics of the oceanic basin since its Oligocene opening and calculated the mean sedimentary rates through time. First attempts on accurate sediment budget calculation were tried by Wu et al. (2018, 2019), but their studied areas were limited in the sub-basins of the SCS, i.e. the

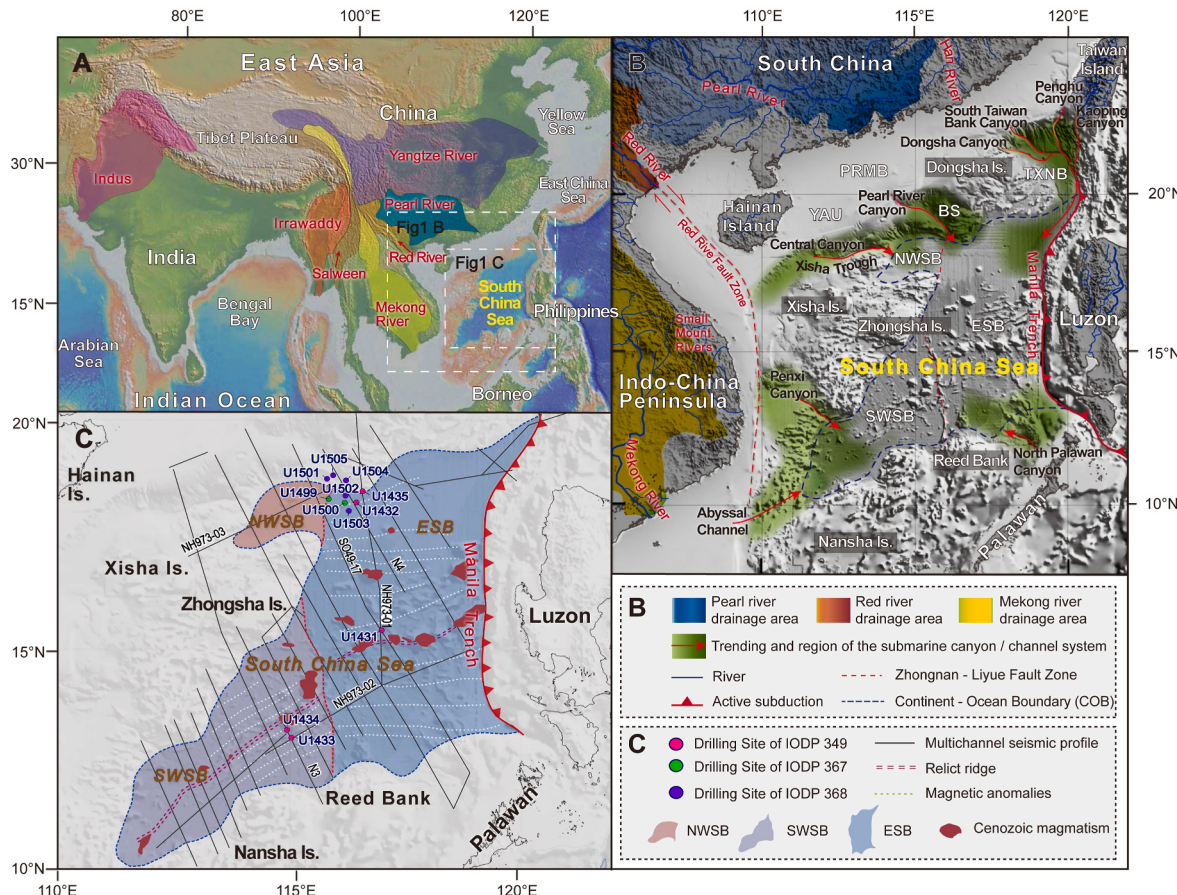


Table 1

Formation time for the major submarine channel/canyon systems surrounding the SCS.

Name	Formation time	References
Dongsha - South Taiwan Bank - Penghu - Kaoping Canyon System Pearl River Canyon	Pleistocene (South Taiwan Bank Canyon: Middle Miocene)	Chen et al. (2020); Yin et al. (2015); Ding et al. (2010); Liu et al. (2019); Chiang et al. (2020); Chuang and Yu, 2002; Ding et al. (2013); Chen et al. (2020); Liu et al., 2019; Huang et al. (2018); Gong et al. (2013); Wang et al. (2017)
Central Canyon (Xisha Trough)	Late Miocene	Ma et al. (2017); Chen et al. (2021); Shao et al. (2019); Su et al. (2014); Chen et al. (2020); Gong et al. (2011); Su et al. (2016)
Penxi Canyon	Late Miocene	Schimanski et al., 2002; Luo et al., 2018; Zhu et al. (2017); Xie et al. (2020)
Mekong River Abyssal Channels	Late Miocene	Guan et al. (2016); Liu et al. (2017b); Huang and Guan (2013)
North Palawan Canyon	Middle Miocene	Yin et al. (2020); Xie et al. (2020)

Table 2

Acquisition parameters for seismic data used in this study.

Seismic Data Series	SO49	N	NH973
R/V	SONNE	TANBAO	TANBAO
Acquisition date	1987	2004	2009
Streamer channel	48	480	480
Record length (s)	12.0	12.0	12.0
Sampling rate (ms)	4	2	2
Shot interval (m)	50	37.5	37.5
Airgun volume (L)	25.6	83.3	83.3

Southwest and Northwest Sub-basins. Their results showed that the sedimentation was generally dominated by regional tectonic events and climate change, but complicated by local tectonic events and geographic position (Wang et al., 2021). However, an accurate quantification of the sediment budget for the whole oceanic basin of the SCS in different geological times has never been done, which definitely hinders a complete reconstruction of sedimentary dispersion and accumulation process in the SCS, as well as the understanding of the interactions between tectonics, climate change, and sea-level changes.

In this study, based on the drilling results from the IODP Expeditions in the SCS, combined with more than 30 multichannel seismic profiles covering the whole oceanic basin (Fig. 1C), we made an age calibration of sedimentary units to reconstruct the Cenozoic sequence stratigraphy framework of the study area, and calculated the sediment budget of the whole oceanic basin of the SCS. We tentatively characterized the million-year-timescale quantification of sediment dispersal and accumulation process of the SCS oceanic basin, and aimed to document the mechanisms controlling the spatio-temporal sediment budget variation, as well as the possible sedimentary provenance.

2. Geological and environmental background

2.1. Geological setting

The SCS has undergone an almost complete Wilson-cycle in Cenozoic, including the continental rifting, seafloor spreading, collision with Borneo in the south, and eastward subduction beneath the Luzon Islands in the east, presenting an complex pattern for three types of continental margins: a passive (rifting) continental margins in the north and south, an active margin (subduction) in the east, and a transform margin in the

west (Fig. 1B; Li et al., 2012).

2.1.1. Geography background

The oceanic basin of SCS is an approximately rhomboid-shaped abyssal basin opening to the east, with the water depth between 3300 m and 4400 m. It is divided into three sub-basins by different geological and geophysical characteristics: the Northwest Sub-basin (NWSB), the East Sub-basin (ESB), and the Southwest Sub-basin (SWSB) (Fig. 1B; Li et al., 2015a; Gao et al., 2019).

The NWSB is the smallest sub-basin with a total width of nearly 200 km and a total length of about 140 km, where the water depth varies between 3500 m and 3700 m (Gao et al., 2021). The NWSB is bounded by the Baiyun Sag and Yitong-Ansha Uplift of the Pearl River Mouth Basin in the north, the Xisha Trough in the west, and the Zhongsha and Xisha Islands in the south. It is separated from the East Sub-basin by the Zhongnan-Liyue Fault Zone (Fig. 1B; Franke et al., 2014; Li et al., 2014).

The ESB is the biggest sub-basin of the SCS with an area of 247, 500 km², separated from the SWSB and NWSB by the Zhongnan-Liyue Fault Zone (Fig. 1B). The eastward subduction of the oceanic crust along the Manila Trench has formed the active continental margin in the east. In the north is a rifted continental margin containing Pearl River Mouth Basin, the Dongsha Islands, the Taixinan Basin, while to the south is the Reed Bank, and the Palawan. The sedimentary layers gradually thinned from the passive continental margins in the south and north to the center of the oceanic basin with the gradually uplifted basement (Ding et al., 2018). Amounts of seamounts lies on both flanks of the extinct spreading center (Li et al., 2011; Zhao et al., 2020).

The SWSB is a V-shaped basin opening to the northeast with an area of 115, 000 km², roughly outlined by the 3000 m isobath, and the water depths between 3000 m and 4000 m. On the north, the Zhongsha Islands separate the SWSB from the NWSB, while the Nansha Islands (Dangerous Grounds) and Reed Bank lie to the south (Fig. 1B). The Indo-China Peninsula borders its west, and the Zhongnan-Liyue Fault Zone separates the SWSB from the ESB in the east (Franke et al., 2014; Ding et al., 2016).

2.1.2. Cenozoic tectonics

Previous studies suggest that the SCS was part of South China during the Mesozoic (Taylor and Hayes, 1983; Hall, 2002). Since the Late Cretaceous, episodic continental rifting occurred as the stress field changed from compression to extension caused by the rollback of the Pacific subduction, which resulted in a series of sedimentary basins in the northern and southern margins of the SCS. Continuous rifting finally leaded to the seafloor spreading in the Early Oligocene and formation of the oceanic basin (e.g. Taylor and Hayes, 1983; Briais et al., 1993; Cullen et al., 2010; Franke et al., 2014).

Shipboard results of microfossil biostratigraphy and palaeomagnetic results from the IODP Expedition 349 (Li et al., 2015b) and the IODP Expeditions 367&368 (Sun et al., 2018), combined with analysis on recently-acquired deep tow magnetic anomalies (Fig. 1C; Li et al., 2014), and ⁴⁰Ar/³⁹Ar dating of basalts near the fossil spreading ridge (Koppers, 2014), have shown that seafloor spreading occurred between ~ 33 Ma and 16 Ma, supporting age models proposed by Taylor and Hayes (1983) and Briais et al. (1993). The seafloor spreading occurred in the ESB and NWSB first, followed by episodic southward ridge jumps at ~ 27 Ma and ~ 23.8 Ma respectively, and the latter jump event resulted in a re-orientation of the spreading geometry from a westward to a southwestward ridge propagation, and the opening of the SWSB (Briais et al., 1993; Ding et al., 2018; Sun et al., 2019). The seafloor spreading ceased in NWSB after the 23.8 Ma ridge jump event (Barckhausen et al., 2014; Cameselle et al., 2017), but continued both in ESB and SWSB before a final cessation at ~ 16 Ma. The cessation time coincided with the onset of collision between Palawan and Borneo and Mindoro-Central Philippines (Clift et al., 2008a, 2008b; Cullen et al., 2010), suggesting a causal relationship between the two events.

Since the Middle Miocene, the SCS has been continuously subducting

eastward beneath the Luzon Islands along the Manila trench. Continuous NNW movement of the Philippine Sea Plate finally triggered the collision between the Luzon Islands and the Eurasian Plate at about 9 Ma, as well as the orogeny of the Taiwan Island in the northeast of the SCS and the closure of the entire oceanic basin of the SCS (Sibuet and Hsu, 2004; Liu et al., 2016). Although the SCS was generally dominated by thermal subsidence since the Miocene, local uplifting events occurred occasionally, such as the uplift of the Dongsha Islands between 13.8 and 2 Ma in the northern continental margin (Lüdmann et al., 2001; Luan et al., 2012; Sun et al., 2014), the uplift of the central Vietnamese plateau at ~8 Ma on the west (Cung et al., 1998; Carter et al., 2000; Miao et al., 2017), and rapid uplift of Borneo during the late Miocene (Rangin et al., 1990; Liu et al., 2016).

2.2. Cenozoic magmatism in SCS

Volcanic seamounts are widely distributed in the oceanic basin of SCS (Fig. 1B). Dredged seamount samples range in ages from ~16 Ma to <1 Ma reveal most of the seamounts were formed after the cessation of seafloor spreading (Yan et al., 2008; Li et al., 2015b; Zhao et al., 2020).

Most of the seamounts in the oceanic basin arranging in chain-like conformation lied along or on the north of the spreading ridge in the ESB and SWSB, some scattered to the northern continental-oceanic transitional zone (Taylor and Hayes, 1980, 1983; Pautot et al., 1990; Li et al., 2002; Zhao et al., 2020). Compared with the whole oceanic basin of the SCS, the seamounts were small in volume, and the pyroclasts were limited produced by denudation and weathering (Huang and Wang, 2006), which had little influence on the calculation results of the sediment budget for the whole oceanic basin of the SCS.

2.3. Asian monsoon

As the major climate feature of the SCS, the alternating summer and winter monsoon winds of the East Asia plays an important role in controlling the climatic and environmental characteristics such as seasonal rainfall, river runoff, and terrestrial material supply, etc. (Webster et al., 1998; Wang et al., 2003).

Substantial evidence suggests that the Asian climate was dominated by monsoon since 24 Ma - 22 Ma (Liu et al., 1998; Sun and Wang, 2005; Clift et al., 2008a, 2008b; Ma and Tian, 2015). During the Neogene, the East Asia was controlled by winter monsoon due to the global temperature changes, especially under the global cooling pattern since ca. 17 Ma (Ma and Tian, 2015; Jiang et al., 2017). The intensity of winter monsoon reached its peak during the Late Miocene (11.6 Ma - 5.3 Ma) (Wan et al., 2007; Holbourn et al., 2018). The East Asian summer monsoon has also been obvious staged since the ~15 Ma: with a strengthened stage from 15 Ma - 11 Ma, a gradually weakened stage during 11 Ma - 4 Ma with increasing winter monsoon, and a strengthened stage again between 4 Ma - 0 Ma (Clift et al., 2008a, 2008b; Ma and Tian, 2015).

In summary, the East Asian summer monsoon prevailed during the Middle Miocene (16 Ma - 11.6 Ma), the Pliocene (5.3 Ma - 1.8 Ma), and Pleistocene to the present (1.8 Ma - 0 Ma), while the winter monsoon prevailed in the Late Miocene (11.6 Ma - 5.3 Ma) over the SCS and its surrounding areas. When dominated by summer monsoon, the climate is warm and humid along with the rainfall increasing, and the runoff of rivers on the continent increased with the transport capacity is strengthened, causing the increase of terrigenous materials transporting to offshore. However, the winter monsoon makes the climate become cold and dry, and the decreasing rainfall further reduces the runoff and transportation capacity of the rivers. The terrigenous debris transported to the offshore would be less.

2.4. Fluvial drainage system around the SCS

The clastic deposits discharged into the SCS were mainly through

numerous river systems in South China, Indo-China Peninsula, Taiwan Island, and Luzon Islands (Fig. 1B), including big rivers such as the Pearl River, the Red River, and the Mekong River, or small rivers with large annual runoff, such as the Chou Shui River and Kao Ping River in southern Taiwan Island (Liu et al., 2008; Huh et al., 2011); small mountainous rivers from the Annamite range in eastern Indo-China Peninsula (Schimanski et al., 2002); small-moderate rivers in western Luzon Islands (Milliman and Syvitski, 1992), and some paleo-rivers that were once with high stream discharge, such as the Han River (Zhang et al., 2012; Zhao et al., 2019), the paleo “Kontum-Ying-Qiong” River system from the Central Vietnam (Shao et al., 2019). These rivers transport more than 700 million metric tons of clastic deposits into the SCS annually, representing 3.7% of estimated global fluvial sediment discharge to the world ocean (Milliman and Farnsworth, 2011; Liu et al., 2016). Developing history of major rivers around the SCS is shown in Figs. 4 and 5.

2.5. Eustatic sea level change of the SCS

Eustatic sea level change plays an important role in sedimentary accumulation process. During the high sea level stage, terrigenous sediments are mainly accumulated on continental shelf, especially near the river mouth; however, when the sea level falls to the shelf break, the continental shelf would be exposed. Rivers would have run across the continental shelf, allowing direct fluvial sediments delivery to abyssal basin.

A Tertiary relative sea level change curve was built by Pang et al. (2005) based on a micropaleontological analysis from 60 exploration wells in the Pearl River Mouth Basin (Fig. 5). The curve demonstrated that the sea level of the SCS area had experienced 16 periods of obvious fluctuation cycles since ~21 Ma. During 23.8 Ma - 10.5 Ma, the decrease of sea level reached the continental shelf break area of the northern SCS eight times, i.e. 23.8 Ma, 21 Ma, 17.5 Ma, 16.5 Ma, 15.5 Ma, 13.8 Ma, 12.5 Ma, 10.5 Ma (Peng et al., 2006). In such regressive events, the continental rivers (such as the Pearl River, Han River) could directly flow through the broad shelf before reaching the continental shelf break area, and transported a large amount of terrigenous materials to the slope and the abyssal basin, thus affecting the sedimentary process in the oceanic basin of the SCS.

2.6. Submarine channel and canyon system

Currently, there are six large submarine channel/canyon systems are formed around the oceanic basin of the SCS as the main conduits for transporting sediments from the continental shelf to the abyssal environment (Fig. 1B; Table 1).

Among them, three canyon systems are distributed along the northern continental margin. From east to west they are: (1) the Dongsha-South Taiwan Bank-Penghu-Kaoping Canyon System (DSPK); (2) the Pearl River Canyon System (PRCS); and (3) the Central Canyon System (CCS). In the DSPK Canyon System, the South Taiwan Bank Canyon was formed during the Middle Miocene at ~13.8 Ma (Ding et al., 2013; Liu et al., 2019), followed by the formation of Penghu and Gaoping Canyon since the Pleistocene (Chen et al., 2020), and the Dongsha Canyon after ~0.9 Ma (Yin et al., 2015). The PRCS began to develop and transport sediments into the oceanic basin since ~21 Ma due to the sudden northward migration of the shelf break (Shao et al., 2004; Ding et al., 2013; Chen et al., 2020). Most scholars believe that the CCS was formed gradually since ~11.6 Ma (Ma et al., 2017; Chen et al., 2021), and then experienced a shrank limitation distribution in the eastern Qiongdongnan Basin due to changes in tectono-sedimentary environment during the Late Pliocene (3.8 Ma - 1.8 Ma). Since the Pleistocene, the CCS revitalized as the climate change and increased the capacity of sediment recharge again (Su et al., 2014, 2016; Shao et al., 2019; Chen et al., 2020).

There are also three large submarine channel/canyon systems in the

western and southern margin of the SCS (Fig. 1B). The Penxi Canyon System (PCS) was formed during the Late Miocene (11.6 Ma - 5.3 Ma) and merges into the SWSB in NW-SE direction (Zhu et al., 2017; Luo et al., 2018). The Mekong River Abyssal Channels (MRAC) lie in the southwest, have become the most important passages transporting terrigenous materials from the Indo-China Peninsula to the SCS since the Late Miocene (Guan et al., 2016; Liu et al., 2017b). The North Palawan Canyon System (NPCS) connected the Palawan and the ESB, incising the southern continental shelf and slope of the SCS. It has undergone at least 20 cycles of canyon incising and infilling since ~15 Ma (Yin et al., 2020).

3. Data and methods

3.1. Data

3.1.1. Multichannel seismic (MCS) data

In this paper, 31 multichannel seismic profiles with a coverage area of $7 \times 10^5 \text{ km}^2$ are chosen to study, including 6 profiles of the SO49 Series obtained during the “Joint Sino-German SONNE 49 Cruise” in 1987; 20 profiles of the N Series obtained during the “National Ocean Project cruise of the Second Institute of Oceanography, Ministry of Natural Resource, China” in 2004; and 5 profiles of the NH973 Series obtained during the “Cruise for Project SCS Continental Margin Geodynamics” in 2009. These multichannel seismic profiles basically covered the whole oceanic basin of the SCS (Fig. 1C), which could effectively control the tectonic and sedimentary change. Detailed acquisition parameters of the seismic profile series are listed in Table 2.

3.1.2. Drill hole data and age calibrations of seismic unit

Since the industrial drilling sites were mainly concentrated on the continental shelf and slope, drilling results from IODP Expedition 349, 367 & 368 were used to interpret seismic sequences and define regional lithostratigraphic units in this study. The well locations and information are shown in Fig. 1C and Table 3. Among them, six wells encountered the basaltic basement (U1431, U1433, U1434, U1500, U1502, U1503). For seismic profiles running through or lying very close to the drilling sites, the lithology and age of both sediments and basements can be well constrained, such as the seismic profiles SO49-17a and NH97303 in the NWSB constrained by Site U1499 (Fig. 2A); the seismic profiles SO49-17b and NH97301 in the ESB constrained by Site U1431 (Fig. 2B); and the seismic profiles N3 and NH97302 in the SWSB constrained by Sites U1433 and U1434 (Fig. 2C). We used these drilling sites to construct the sequence stratigraphic framework (Fig. 2). Stratigraphic interface dating was mainly obtained through biostratigraphic analysis data by Li et al. (2015b) and Sun et al. (2018). Some seismic profiles provided tie cross lines for correlation of dated horizons between NW-SE orientation main profiles, such as the seismic profile NH97302 in SWSB (Fig. 2C), and the NH97303 in NWSB (Fig. 2A). In this study, we distinguished six

distinct sedimentary units in Cenozoic sediments corresponding to distinct tectono-sedimentary environments, i.e. the Oligocene, the Lower Miocene, the Middle Miocene, the Upper Miocene, the Pliocene, and the Pleistocene, from bottom to top respectively (Fig. 2).

3.2. Calculation of sediment budget

Due to the uneven distribution and large spacing of the IODP drilling sites in the study area, which has limited constraints on lithology, we use the simplified calculation formula proposed by Clift (2006) to calculate the sediment budget:

$$\Delta R = V_{\Delta t} / \Delta t$$

where ΔR stands for the sediment budget of a certain period of geological time (in km^3/my), $V_{\Delta t}$ is the total volume of sediments in the certain geological period (in km^3), and Δt is the duration time of the geological period (in my).

3.2.1. Time-to-depth conversion and decompaction process

The calculation of the sediment budget involves time-to-depth conversion and decompaction process of the interpreted seismic sections. Logging data of the Site U1431 in the ESB, Site U1433 in the SWSB, and Site U1499 in the NWSB provided accurate time-to-depth conversion information, which are as follows:

$$\begin{aligned} \text{In ESB: } Z &= 0.000188295 t^2 + 0.695896 t \text{ (Li et al., 2015b);} \\ \text{In SWSB: } Z &= 0.000152626 t^2 + 0.714658 t \text{ (Li et al., 2015b);} \\ \text{In NWSB: } Z &= 0.0003 t^2 + 0.5659 t \text{ (Sun et al., 2018);} \end{aligned}$$

Where, t stands for the two-way travel time starting from the seafloor (in milliseconds), and Z is the depth in meters below the seafloor (mbsf).

Compaction of sediments is related to their porosity and lithology. After time-depth conversion, we decompacted each sedimentary unit to obtain the original thickness using the program *Flex-Decomp™* by Kusznir et al. (1995), whose study developed mathematical forward models of rifting, and applied to both syn- and post-rift stages of basin evolution to restoring compaction processes. During the decompaction process, the loss of porosity of each sedimentary unit was estimated. In this study, we constrained the decompaction process with lithology information from Sites U1502, U1433, and U1431. These three drilling sites distribute in three sub-basins of the SCS respectively, which drilled into the basaltic basement and could provide a complete porosity and lithology information of the Cenozoic strata (Li et al., 2015b; Sun et al., 2018).

3.2.2. Grid data generation and sediment volume calculation

After we got the uncompacted thickness of each sedimentary unit, we used the *Surfer* software for the grid data generation and sediment

Table 3

Drilling Sites of the IODP 349, 367 & 368 Expedition used in this study.
(Li et al., 2015b; Sun et al., 2018; Jian et al., 2018; W Wang et al., 2019).

Expedition	Site	Northern Latitude	East Longitude	Tectonic Domain	Deepest Age	Deepest Lithology
IODP 349	U1431	15°22'	117°00'	ESB	Early Miocene	Basalt
	U1432	18°21'	116°23'	ESB	Pleistocene	Clay
	U1433	12°55'	115°02'	SWSB	Early Miocene	Basalt
	U1434	13°11'	114°55'	SWSB	Middle Miocene	Basalt
	U1435	18°33'	116°36'	COT	Pre-Oligocene	Clay and silty sand stone
IODP 367	U1499	18°24'	115°51'	NWSB	Oligocene	Breccia
	U1500	18°27'	116°13'	ESB	Oligocene	Basalt
IODP 368	U1501	18°53'	115°46'	COT	Mesozoic	Sand stone
	U1502	18°27'	116°14'	COT	Oligocene	Basalt
	U1503	18°08'	116°19'	ESB	Oligocene	Basalt
	U1504	18°50'	116°14'	COT	Eocene (?)	Calc-silicate schist with granofels clasts
	U1505	18°55'	115°51'	COT	Oligocene	Clay and silty sand stone

COT: continent-ocean transition zone.

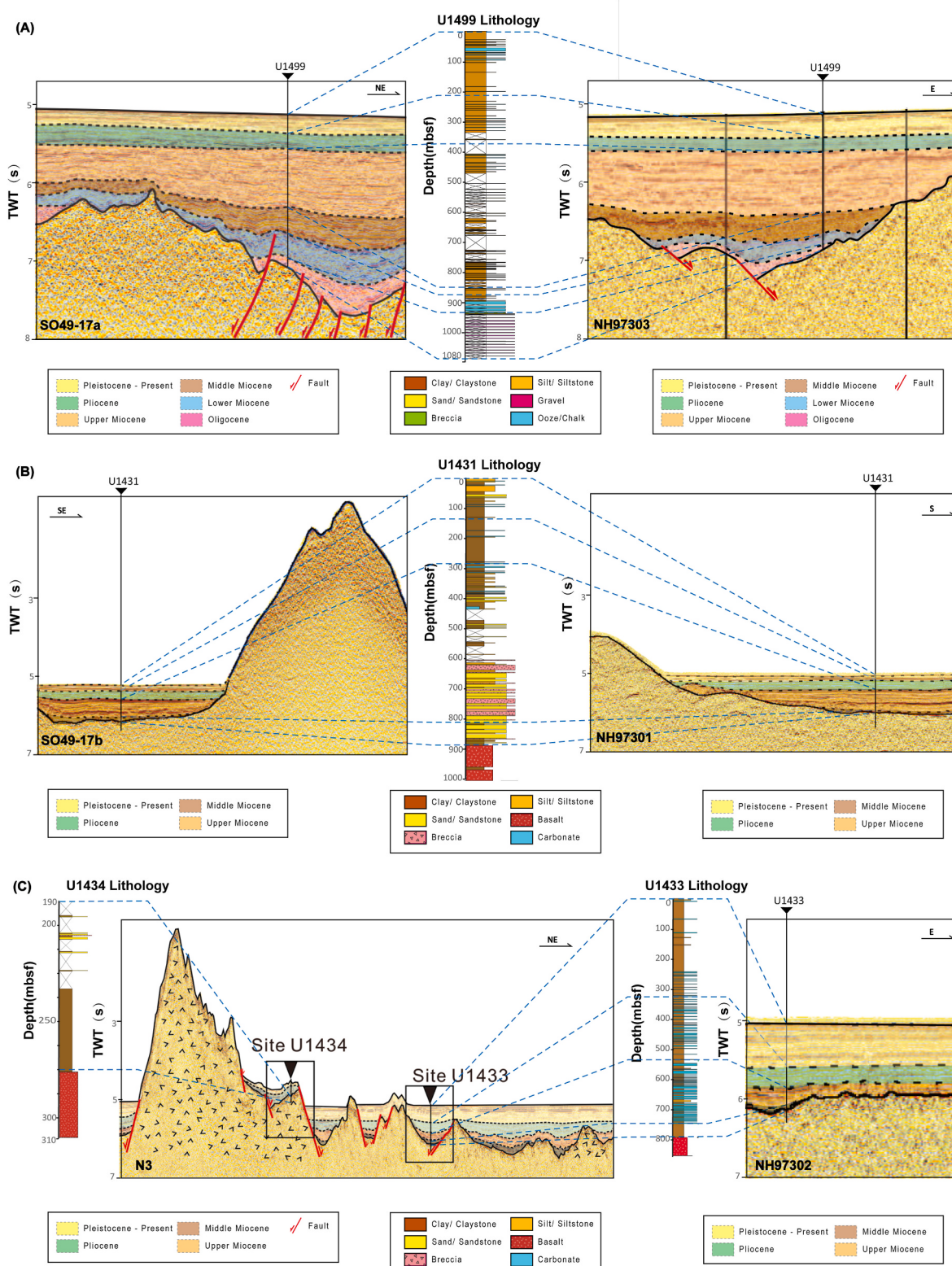


Fig. 2. Drill hole data and age calibrations of seismic units. (A) Calibration of seismic units in seismic profiles SO49-17a and NH97303 from lithostratigraphy at Site U1499 in the NWSB. Site U1499 is located in the continent-ocean transition zone of the SCS. At Site U1499, the basaltic basement was not penetrated but most Cenozoic sediments have been recovered. (B) Seismic profiles SO49-17 b and NH97301 in the ESB constrained by Site U1431. (C) Calibration of seismic units in seismic profiles N3 and NH97302 from recovered lithostratigraphy at Site U1433 and Site U1434 in the SWSB. Site U1431 and Site U1433 are located near the spreading ridges, and penetrated the basaltic basement and acquired whole core samples from sedimentary strata above the basement. Drilling sites and seismic profiles distribution are shown in Fig. 1(B). The interpreted boundaries are calibrated from recovered lithostratigraphic units, which were mainly obtained through biostratigraphic analysis data by Li et al. (2015b) and Sun et al. (2018).

volume calculation of the oceanic basin at different times. By importing the unloaded and decompacted depth of each sedimentary boundary into the software, the interface grid data can be generated and followed by a planar graph (Fig. 3). Longitude and latitude data from each seismic profile are also used to directly constrain the surface area of the oceanic basin. The sediment volume between two sequence boundaries can be finally determined by computing the grid volume in between.

3.2.3. Error analysis

The calculation results of sediment budget in this paper may have errors in the following three aspects:

- (1) Errors caused by the time-to-depth conversion process. Although Li et al. (2015b) found that the stratigraphic depths of U1431 and U1433 near the relic spreading ridge of ESB were almost the same after their respective time-depth conversions in different sub-basins, but they would have deviated gradually with increasing depths from those obtained at Site U1432 located in the north and Site U1435 on the northern continent-ocean transition zone (COT). Hence, the time-depth conversion error is assumed to be 3%.
- (2) Errors in age calibrations, lithology and porosity estimation during the decompaction process. Errors in estimating the sediment age, lithology, and compaction history rarely exceed 2% (Clift, 2006), since they were provided directly from the latest IODP drilling results. Due to better drilling control and the high fitting accuracy, we adopted a 2% error value (Lei et al., 2015; Wu et al., 2019).
- (3) The ideal method for calculating sediment budgets is to use the 3D seismic data with full coverage of the oceanic basin. Due to the limited coverage of the 2D survey seismic lines, there are certain errors in the process of the top and bottom interfaces of different sedimentary units obtained by interpretation. In this study a maximum 5% error was estimated followed Clift (2006), Ding et al. (2016) and Wu et al. (2019).

Therefore, in this study, the total error range for the calculation results of sediment budget was set as $\pm 10\%$.

3.3. Cenozoic sediment isopach mapping

Horizon grids in depth (km), sediment thickness (isopach) grids for

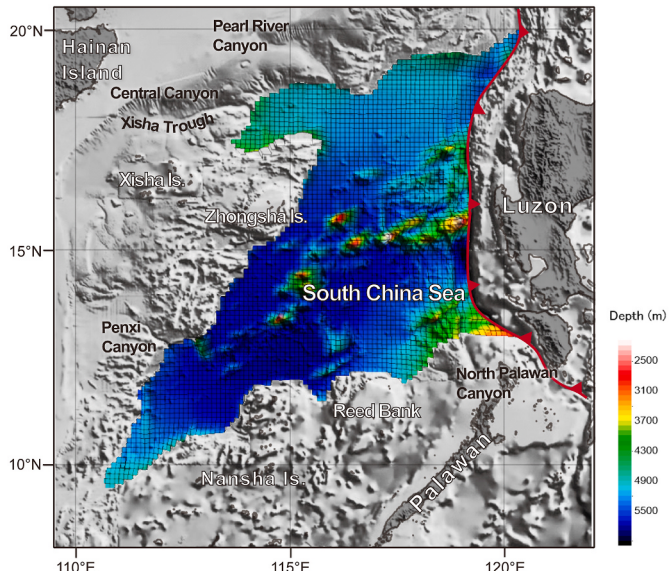


Fig. 3. Grid data model and planar graph of the seafloor.

each unit were calculated using professional seismic interpretation software *Geo-Frame* and geological mapping software *Surfer* by importing the unloaded and decompacted depth of each sedimentary boundary into the software and interpolating by the kriging algorithm.

Before the sediment isopach maps of the oceanic basin of the SCS were generated, a restoration of the SCS in different geological periods was necessary. This simplified reconstruction of the oceanic basin was conducted by stepwise cutting out the portions of oceanic crust that had formed in the respective time intervals based on the interpreted recently-acquired deep tow magnetic anomalies by Li et al. (2014) (Fig. 1C), and then repositioning the remaining parts along the cutting line. The position of the COB is generally followed Briais et al. (1993), but was modified based on recently published works on the COT, which were combined with seismic data and IODP drilling results (e.g. Larsen et al., 2018; Ding et al., 2020; Nirrengarten et al., 2020). While for the position of continental margin, especially the southern continental margin was based on previous plate kinematic reconstructions (e.g. Li et al., 2015a; Sibuet et al., 2016; Ding et al., 2016). Palaeo-coast line and palaeo-sedimentary environmental reconstructions of the continental margin was followed by Collins et al. (2017), and some details were modified according to Yu et al. (2016), Xie et al. (2006, 2019), and Xie et al. (2021). Isopach maps of six geologic sediment units since the seafloor spreading of the SCS, i.e. the Oligocene and Lower Miocene, the Middle Miocene, the Upper Miocene, the Pliocene, and the Pleistocene, were reconstructed and shown in Fig. 4A–F.

4. Results

In this section we describe the calculation results of the Cenozoic sediment budgets for the three sub-basins and the whole oceanic basin of the SCS by adding them together, which could quantitatively describe the sedimentary process of the SCS (Table 4). Dispersion and accumulation characteristics of the terrigenous sediments in different epochs were also documented based on the Cenozoic sediment isopach maps (Fig. 4A–F).

4.1. Cenozoic sediment budget of the oceanic basin, SCS

ESB: As shown in Table 4, the sediment budget of the ESB is $2.86 \times 10^3 \text{ km}^3/\text{my}$ from the Oligocene to the Early Miocene (33 Ma - 16 Ma), and increases rapidly to $6.93 \times 10^3 \text{ km}^3/\text{my}$ during the Middle Miocene (16 Ma - 11.6 Ma), followed by a gradually increase to $10.63 \times 10^3 \text{ km}^3/\text{my}$ during the Late Miocene (11.6 Ma - 5.3 Ma). Since the Pliocene (5.3 Ma - 1.8 Ma), there is an apparently increase to $12.17 \times 10^3 \text{ km}^3/\text{my}$ in the ESB, and reaches its peak since the Pleistocene (1.8 Ma - 0 Ma) with a value of $34.11 \times 10^3 \text{ km}^3/\text{my}$, being almost three times as much as the previous period.

NWSB: The sediment budget in the NWSB starts from $0.75 \times 10^3 \text{ km}^3/\text{my}$ from the Oligocene to the Early Miocene (33 Ma - 16 Ma), and increases to $1.57 \times 10^3 \text{ km}^3/\text{my}$ during the Middle Miocene (16 Ma - 11.6 Ma). It reaches its peak to $2.61 \times 10^3 \text{ km}^3/\text{my}$ in the Late Miocene (11.6 Ma - 5.3 Ma). Since the Pliocene (5.3 Ma - 1.8 Ma) there is an obvious decline to $1.53 \times 10^3 \text{ km}^3/\text{my}$, and then increases again (up to $2.39 \times 10^3 \text{ km}^3/\text{my}$) since the Pleistocene (1.8 Ma - 0 Ma), which is much lower than that of the ESB and NWSB.

SWSB: The sediment budget in the SWSB shows a wavy curve in general. In the Early Miocene (23 Ma - 16 Ma) it is $0.77 \times 10^3 \text{ km}^3/\text{my}$, then increases rapidly to $5 \times 10^3 \text{ km}^3/\text{my}$ during the Middle Miocene (16 Ma - 11.6 Ma). During the Late Miocene (11.6 Ma - 5.3 Ma) we witness a slightly decrease to $4.65 \times 10^3 \text{ km}^3/\text{my}$, but it increases again after the Pliocene (5.3 Ma - 1.8 Ma) to $7.62 \times 10^3 \text{ km}^3/\text{my}$. Like the ESB, the sediment budget reaches its peak of $24.14 \times 10^3 \text{ km}^3/\text{my}$ since the Pleistocene (1.8 Ma - 0 Ma).

Whole SCS Oceanic Basin: The sediment budget of the whole SCS Oceanic Basin is obtained by adding the data of the three sub-basins. It is $4.38 \times 10^3 \text{ km}^3/\text{my}$ between the Oligocene and the Early Miocene (33

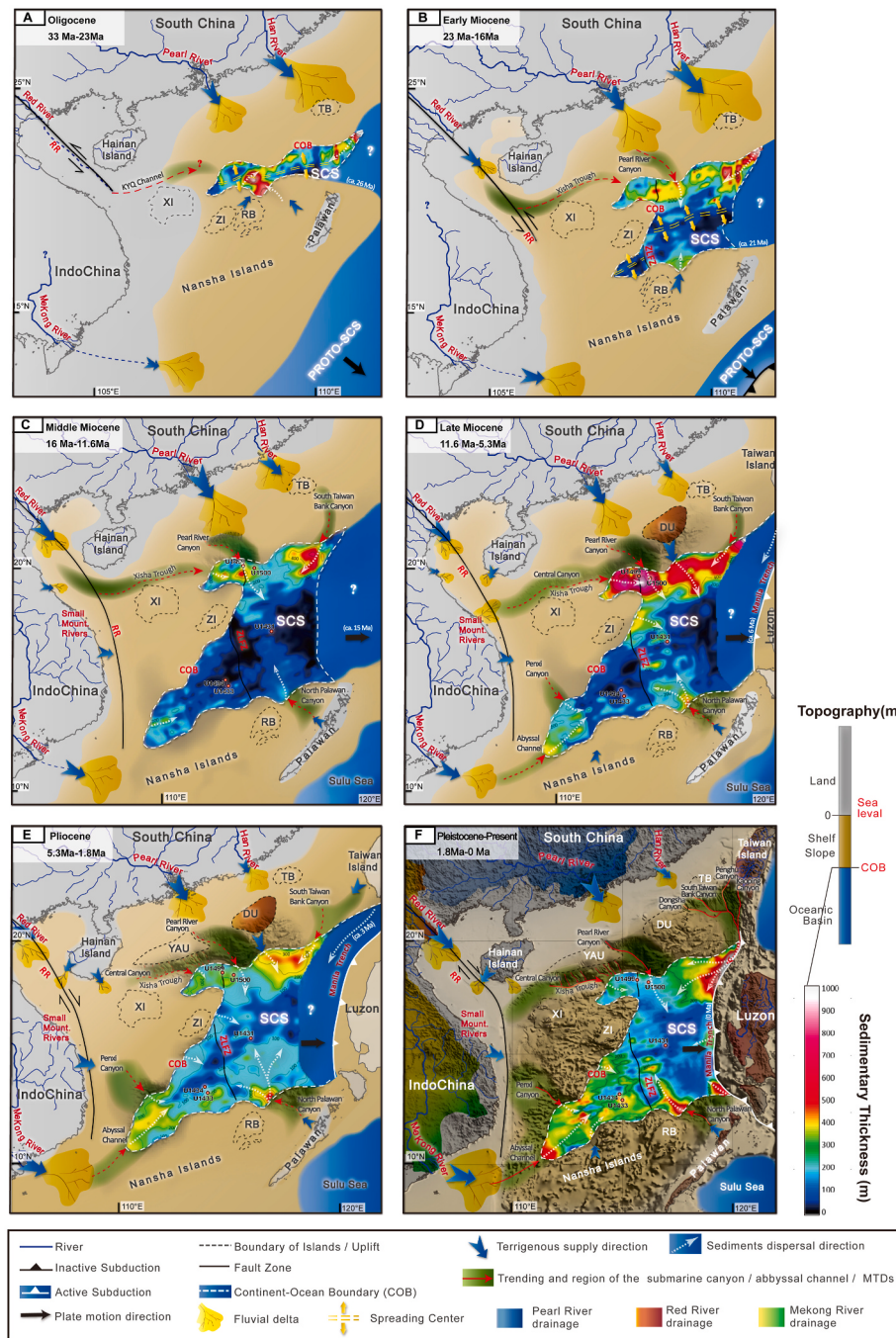


Fig. 4. Sedimentary evolution reconstructions of the SCS based on sediment isopach mapping for six geological time: (A) Oligocene (33 Ma - 23 Ma); (B) Early Miocene (23 Ma - 16 Ma); (C) Middle Miocene (16 Ma - 11.6 Ma); (D) Late Miocene (11.6 Ma - 5.3 Ma); (E) Pliocene (5.3 Ma - 1.8 Ma); (F) Pleistocene (1.8 Ma - 0 Ma). The sedimentary isopach maps and white dotted arrows indicate the distribution characteristics and the dispersal and accumulation process of terrigenous sediments in the SCS oceanic basin, respectively.

The boundary restoration of the SCS oceanic basin in different geological periods was based on the interpreted recently-acquired deep tow magnetic anomalies by Li et al. (2014) (shown in Fig. 1C) and the COB/COT position followed by published works (e.g. Briais et al., 1993; Larsen et al., 2018; Ding et al., 2020; Nirrengarten et al., 2020). The position of continental margin was based on previous plate kinematic reconstructions (e.g. Li et al., 2015a; Sibuet et al., 2016; Ding et al., 2016). Palaeo-coast line and palaeo-sedimentary environmental reconstructions of the continental margin was followed by Yu et al. (2016); Collins et al. (2017); Xie et al. (2006, 2019, and Xie et al. (2021). The evolution of the Pearl River, Red River, Mekong River, and Han River were based on Zhang et al. (2012); Zhao et al. (2015); Chen et al. (2017); and Cao et al. (2018), etc.; The references for the formation age of the major submarine channel/canyon systems surrounding the SCS were listed in Table 1.

XI, Xisha Islands; ZI, Zhongsha Islands; RB, Reed Bank; TB, Taiwan Bank; DU, Dongsha Uplift; YAU, Yitong - Ansha Uplift; KYQ, Kontum-Ying-Qiong Channel (Shao et al., 2019); ZLFZ, Zhongnan-Liyue Fault Zone; RR, Red River Fault Zone; COB, Continent-Ocean Boundary.

Ma - 16 Ma), and increases rapidly to $13.50 \times 10^3 \text{ km}^3$ in the Middle Miocene (11.6 Ma - 5.3 Ma). During the Late Miocene (11.6 Ma - 5.3 Ma) the value increases gradually to $17.90 \times 10^3 \text{ km}^3/\text{my}$, and increases again to $21.32 \times 10^3 \text{ km}^3/\text{my}$ during the Pliocene (5.3 Ma - 1.8 Ma). Nevertheless, a sudden increase and accumulating with the sediment budget to $60.64 \times 10^3 \text{ km}^3/\text{my}$ since the Pleistocene (1.8 Ma - 0 Ma), almost three times as much as the previous period.

4.2. Cenozoic sedimentary isopach mapping reconstruction of the oceanic basin, SCS

During the Oligocene (33 Ma - 23 Ma), the SCS has just started seafloor spreading, either the ESB or the NWSB was in a small scale (Fig. 4A). In general the thickness of the sediment ranges between 100 m and 400 m. Two deposition centers are observed in the northeastern and

southwestern parts, which are close to the Taiwan Bank in the northern continental margin, and Reed Bank and Zhongsha Islands in the south respectively. The thickness of the latter can reach to 1000 m.

During the Early Miocene (23 Ma - 16 Ma), the SCS experienced a southward ridge jump event, and the SWSB began its spreading in a NE-SW propagated pattern (Ding et al., 2016). The sediment is generally featured with a decreasing trend from the slope foot ($>1000 \text{ m}$) to the spreading ridge ($\sim 50 \text{ m}$), which is much thicker in the northern flank than that in south (Fig. 4B). Two major deposition centers could be discovered near the slope foot area in the northeast and northwest parts of the oceanic basin. The former is more than 1000 m in thickness, lying in the downstream area of the Han River delta. The latter lies in the mouth of the Pearl River Canyon system, and the thickness is much lower (between 200 m and 400 m). One depocenter exists in the southern flank, lying just in the slope foot of the Reed Bank. However,

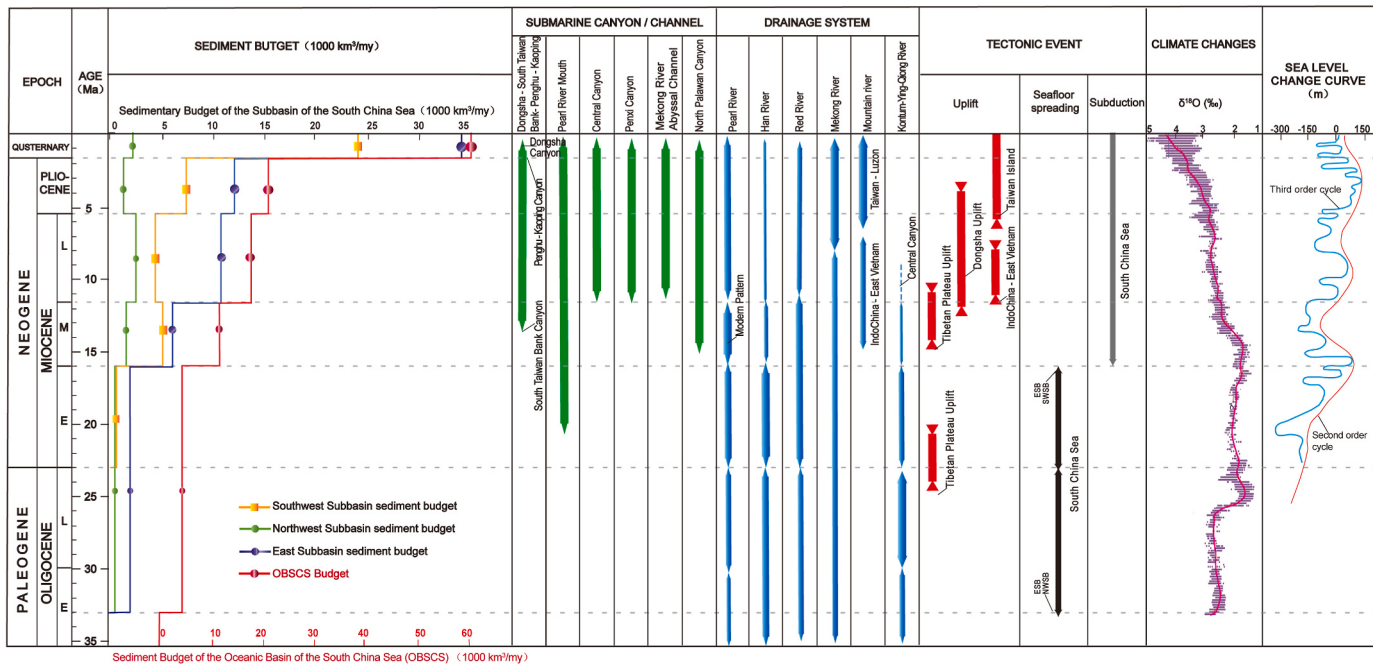


Fig. 5. Sediment budget changes of the SWSB, NWSB, ESB, and the whole oceanic basin of the SCS (OBSCS), as well as the combination of the controlling factors for the “Source-to-Sink” sedimentary process in SCS. Controlling factors include the major submarine channel/canyon systems (Table 1), the drainage system input the SCS (Zhang et al., 2012; Zhao et al., 2015; Liu et al., 2016; Chen et al., 2017; Cao et al., 2018), with the width of the blue band indicated the mass of the river runoff; the major tectonic events occurred both in and around SCS (Li et al., 2015b; Sibuet et al., 2016; Ding et al., 2016), climate changes indicated by the $\delta^{18}\text{O}$ curve (pink line) and the global deep-sea oxygen isotope records (purple squares, from Zachos et al., 2001), and the sea level change curve of the SCS area from Pang et al. (2005).

the thickness is much lower than those in the north, ranging between 150 m and 300 m (Fig. 4B). In the SWSB the sedimentary thickness is generally low (<100 m), except slope foot areas of the Zhongsha Islands and Reed Bank.

During the Middle Miocene (16 Ma - 11.6 Ma), the seafloor spreading both ceased in the ESB and SWSB. The whole oceanic basin was generally dominated by thermal subsidence (Wang et al., 2021), providing a vast space for sediment. The sediment in the northern flank is generally over 100 m, which can reach up to ~500 m in the center of the NWSB and northeastern part, forming three depocenters (Fig. 4C). All these depocenters just lie in the mouth of the submarine canyon systems, including the South Taiwan Bank Canyon, the Pearl River Canyon, and the Center Canyon from east to west. The correspondence between depocenters and submarine canyon systems indicate the strong terrigenous sediment transportation capability of the latter. The sediment is much thinner in the center and southern part of the oceanic basin, ranging between 100 m and 150 m. Depocenters are limited in the downstream regions of the submarine channel/canyon systems, such as the North Palawan Canyon in the southeast. The thickness can reach to ~200 m (Fig. 4C).

During the Late Miocene (11.6 Ma - 5.3. Ma), the SCS began its eastward subduction beneath the Luzon Islands since ~9 Ma (Liu et al., 2020). A sharp increase in sedimentation occurred almost throughout the basin (Fig. 4D). The locations of depocenters still mainly focused on the slope foot of the northern flank, as well as the whole NWSB, but the thickness increases sharply, generally being higher than 500 m. These depocenters also generally lie in the mouth of submarine channel/canyon systems, including the South Taiwan Bank Canyon, the Pearl River Canyon, and the Central Canyon from east to west (Fig. 4D). Other depocenters include the one in the slope foot east of the Zhongsha Islands (>100–400 m), the one in the mouth of the North Palawan Canyon (>100 m–500 m) in the south, and the one in the mouths of Penxi Canyon and Mekong River Abyssal Channels in the southwest corner. But the thickness is much lower than those in the north (Fig. 4D).

During the Pliocene (5.3 Ma - 1.8 Ma), the sedimentation decreased a lot both in the NWSB and adjacent mouth area of the Pearl River Canyon (Fig. 4E). The sediment is generally sheet-like without obvious depocenter, although a remarkable depocenter still exists in the northeastern part, or of the slope foot of the Dongsha Uplift, with the thickness reaching to 450 m (Fig. 4E). The sedimentation in the central part of the oceanic basin increases, with the average thickness ranging between 150 m and 200 m, indicating a ridgeward sediment dispersion. Limited sedimentation occurred in basement highs or seamount chains along the relic spreading ridge. Compared to the slope foot area in the northern part, either the range or thickness of the depocenters in the southern part increases, such as the southeastern one lying in the mouth of North Palawan Canyon, and the one in the southwest corner. The thickness is generally >300 m.

Since the Pleistocene (1.8 Ma - 0 Ma), the thickness of sediments in the northern flank decreases while that in the southern flank increases continuously. The depocenters mainly concentrate on the mouth area of the submarine channel/canyon systems developed in the southern continental margin, including the Mekong River Abyssal Channels in the southwest corner, and the North Palawan Canyon in the south. An exception is the obvious NE-SW trending depocenter along the NE Manila Trench near the Taiwan Island, showing a sediment dispersion from offshore Taiwan (>1000 m) to the abyssal basin (Fig. 4F).

5. Discussion

Fig. 5 is a combination of calculation results of sediment budget, the development history of submarine channel/canyon systems, the river systems around the SCS, the major tectonic events occurred both in and around SCS, the $\delta^{18}\text{O}$ curve indicating the climate change, as well as the sea level change curve of the SCS, enabling us to reconstruct the Cenozoic sedimentary history of the SCS, analysis the controlling factors related with regional and local tectonic activities, Asian monsoon, sea level change, etc., and to complete the final piece in the puzzle on the

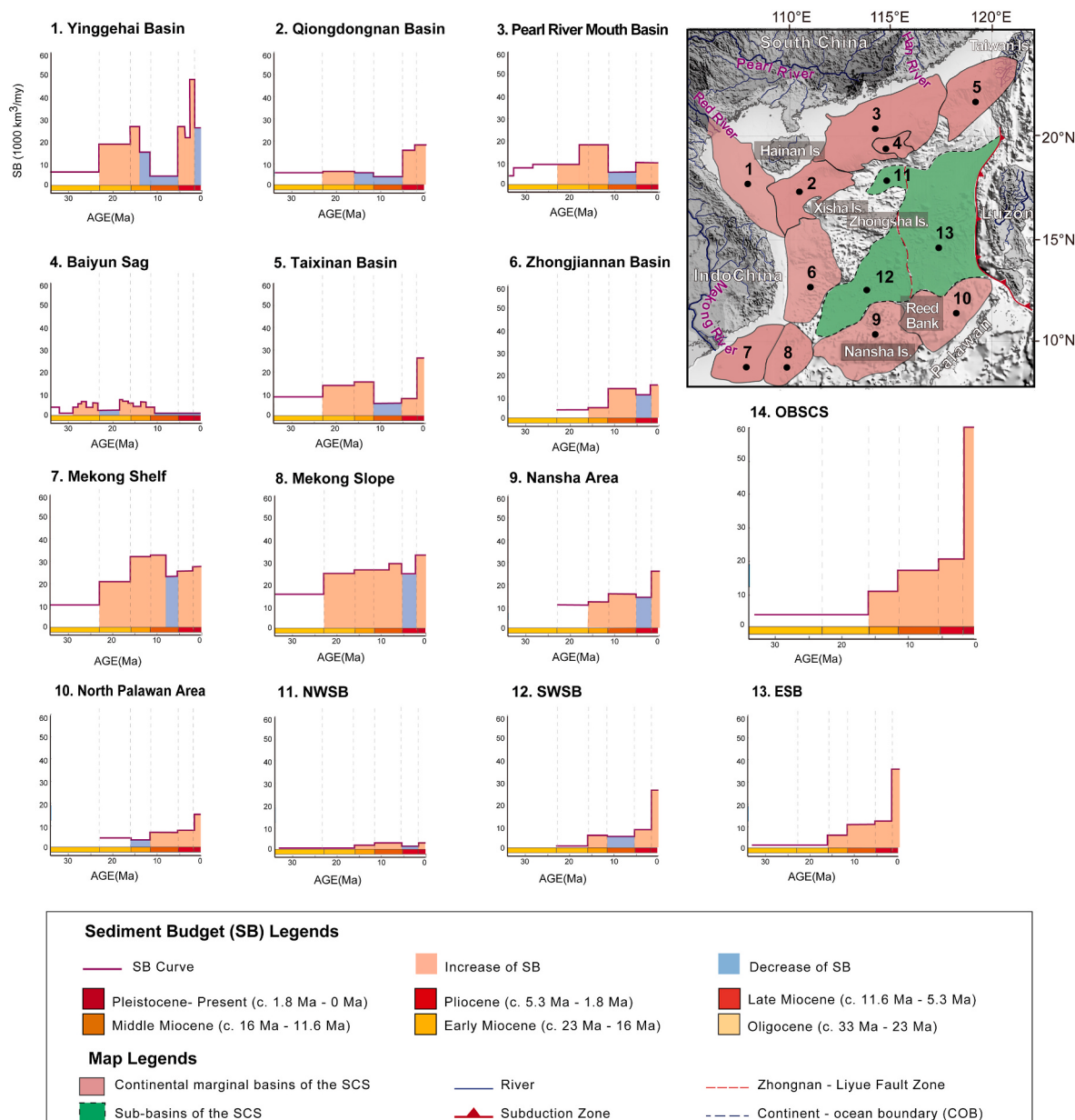


Fig. 6. Simplified comparison of sediment budget trends displaying evidence for quantitative recording the sediments dispersal and accumulation evolve in major sedimentary regions of the SCS. The light red boxes in the background of the curves represents the increase of the sediment budget, and the light blue boxes represents the decrease interval. Pearl River Mouth Basin and Mekong Shelf (Clift, 2006); Baiyun Sag (Xie et al., 2013); Qiongdongnan Basin and Yinggehai Basin (Clift and Sun, 2006); Mekong Slope (Li et al., 2012); Taixinan Basin, Zhongjiannan Basin, Nansha and North Palawan Area (Huang and Wang, 2006); SWSB: Southwest Sub-basin; NWSB: Northwest Sub-basin; ESB: East Sub-basin; OBSCS: Oceanic Basin of the South China Sea (results from Table 2); SB: sediment budget (1000 km³/my).

Table 4

The Calculation results of the sediment budget.

Time	Time Period (Ma)	Duration (m.y.)	ESB		NWSB		SWSB		OBSCS	
			SV	SB	SV	SB	SV	SB	SV	SB
Pleistocene	1.8-0	1.8	61.40	34.11	4.30	2.39	43.46	24.14	109.16	60.64
Pliocene	5.3-1.8	3.5	42.59	12.17	5.36	1.53	26.67	7.62	74.62	21.32
Late Miocene	11.6-5.3	6.3	66.98	10.63	16.47	2.61	29.30	4.65	112.75	17.90
Middle Miocene	16-11.6	4.4	30.47	6.93	6.93	1.57	22.01	5.00	49.40	13.50
Early Miocene	23-16	7	48.67	2.86	12.67	0.75	5.36	0.77	76.71	4.38
Oligocene	33-23	10								

SV: Sediment Volume (1000 km³); SB: sediment budget (1000 km³/my).

“Source-to-Sink” process in SCS. The dispersion and accumulation history in different epochs was also discussed based on the Cenozoic sediment isopach maps (Fig. 4A–F) and the sediment budgets evolution in continental margin of the SCS (Fig. 6).

5.1. Cenozoic sediments accumulation and dispersion process and controlling factors of the oceanic basin, SCS

5.1.1. Oligocene (33 Ma - 23 Ma)

Micro-paleontological studies of numerous industrial wells in the Pearl River Mouth Basin showed that most of the continental shelf in the SCS was in neritic sedimentary environment during the Late Eocene (Pang et al., 2005). Studies on the foraminifera in the drilled sediments of Sites U1501 and U1504, which are located in the Outer Margin High of the SCS confirmed that the continental break-up and initial seafloor spreading occurred in a deep-water environment (Jian et al., 2019). Since the Early Oligocene the ESB and NWSB began the seafloor spreading. The terrigenous sediments transported through the Pearl River and Han River systems in South China were mainly accumulated in the river mouth area of the continental shelf, thus the whole sediment budget in the oceanic basin was relatively low. As the seafloor spreading continued, rapid subsidence occurred in the Baiyun Sag during 29 Ma - 23 Ma, which lies in the south of the Pearl River Mouth Basin, which not only caused a northward migration of the continental shelf break, but also accommodated a large amount of sediments imported into the ocean via the Pearl River (Ding et al., 2016; Fang et al., 2022). According to the geochemical and Nd isotope data of the northern SCS, the Pearl River system gradually expanded westward from a small-scale water system limited to the coast in the early Oligocene to a large-scale water system covering most of South China in the Early Miocene, gradually controlling the regional sediment supply of the Pearl River Mouth Basin (Shao et al., 2016; Cao et al., 2018; P. Wang et al., 2019; Ma et al., 2019). However, the sediments were mainly accumulated in the continental slope area except entering the oceanic basin. That explains why the sediment budget in the Pearl River Mouth Basin increase during this period (Clift, 2006; Xie et al., 2013), while that in the SCS oceanic basin was relatively low. In addition to the sediment carried by the rivers, the IODP drilling sites in the continent-ocean transition zone and initial oceanic crust of the northern SCS, such as Site U1499, encountered less than 150 m of deposits of this period (Fig. 2A). The local depocenters are all close to the basement highs in the continental shelf, such as the Zhongsha Islands, the Reed Bank and the North Palawan Block in the south; and the Taiwan Bank in the northeast (Fig. 4A). We speculated that these depocenters are related to the weathering and denudation of these basement highs.

5.1.2. Early Miocene (23 Ma - 16 Ma)

During the Early Miocene, the spreading ridge jumped southward, resulting in the cessation of the NWSB and the opening of the SWSB. The sediment budgets of most sedimentary basins in the continental margin of the SCS area increased significantly (Total increase over 30.0×10^3 km 3 /my) during this stage, including the Yinggehai Basin, the Pearl River Mouth Basin, the Taixinan Basin in the northern continental margin, and the Mekong Shelf and Slope Area in the west (Fig. 6; Huang, 2004; Clift and Sun, 2006; Clift, 2006; Xie et al., 2013). Since the global glacial climate did not change a lot during the Early-Middle Miocene (Zachos et al., 2001), the enhanced continental denudation during this period might not be related to the climate, but reflected the intensification of denudation in the southeastern Tibet Plateau (Lavé and Avouac, 2001; Finlayson et al., 2002; Clift et al., 2004). Therefore, the increase of sediment budgets in the continental margin of the SCS during the Early Miocene was mainly related to the uplift of the Tibetan Plateau, as well as the southeast extrusion of the Indo-China blocks and enhanced denudation (Wang et al., 2012, 2022; Sun et al., 2015).

Compared with the significant increase in the sediment budget of the continental margin, the SCS ocean basin was generally at a lower level

(Fig. 6). The eustatic curve showed that the sea level gradually increased during the Early Miocene (Fig. 5), and most of the terrigenous sediments were preferentially deposited in the rifted basins in the continental shelf. While for sediments imported into the ocean basin were mainly accumulated at the slope foot, and the thickness gradually decreased from the edge of the ocean basin to the spreading ridge (Fig. 4B). Drilling results of Sites 1148 and U1505 in the slope foot area of ESB shows that the sedimentation rates in the Early Miocene increased by ~10 cm/k.y. and ~8 mm/k.y., respectively, compared with the Late Oligocene (Prell et al., 2006; Sun et al., 2018). However, for the Site U1431 locating near the spreading ridge of the ESB, the sediments in this period had only less than 4 m of clay deposits (Li et al., 2015b). It indicated that the terrigenous sediments in the Early Miocene (23 Ma - 16 Ma) were mainly originated from the northern continental margin, and dispersed to the central basin.

There are two depocenters in the northern flank of the SCS oceanic basin. Compared with the Oligocene period, the depocenter located in the lower reaches of the Han River delta in the northeast was further expanded (Fig. 4B). The other depocenter was located at the mouth of the Pearl River Canyon system. Based on the distribution characteristics and discriminant analysis of rare earth elements of the sediments, Zhang et al. (2012) suggested that the influence range of the Han River was further expanded during the Early Miocene, and the Pearl River submarine canyon also began to develop during this period (Ding et al., 2013; Cao et al., 2018). Although the sea level showed an overall upward trend, there were still two relative sea level drop events at around ~21 Ma and ~17 Ma (Pang et al., 2005). The terrigenous materials carried by the Pearl River and the Han River might have directly crossed the exposed continental shelf and entered the SCS oceanic basin through the submarine channel/canyon systems, forming these two local depocenters. A sedimentary belt with a thickness of about 300 m strips can also be observed in the NWSB (Fig. 4B), which is speculated to be related to material input from the KYQ River to the basin.

The sediment budget of the SWSB was also at a low level in this stage (Fig. 6), and the drilling results of Site U1433 near the spreading ridge showed that the sediment thickness at this stage was less than 50 m (Fig. 2; Li et al., 2015b). The only depocenter in the southern flank was located at the slope foot near the Reed Bank, which might be related to the local denudation.

5.1.3. Middle Miocene (16 Ma - 11.6 Ma)

During the Middle Miocene, the seafloor spreading ceased, and except the east part, the current topographical pattern of the SCS basin was basically formed. The entire ocean basin was generally dominated by thermal subsidence, which provided a broad space for sediment accumulation. The sediment budgets of the continental margin increased continuously (Fig. 6), which could be attributed to the uplift event of the Tibet Plateau and intensification of the East Asian summer monsoon (Clift et al., 2016), as well as the extrusion of related blocks (Including Indo-china and other blocks) to the southeast (Clark et al., 2005), causing massive input of terrigenous materials to the sea due to enhanced denudation. At this stage, The Han River gradually retreated (Zhang et al., 2012), while the runoff of the Pearl River significantly increased, which replacing the Han river as the major river system in the northern SCS. The sediment budget of the whole SCS oceanic basin also showed a rapid increase about 9.12×10^3 km 3 /my, which were still concentrated in the northern flank of the basin (Fig. 4C).

The SCS also experienced multiple sea level decline events during the Miocene (Pang et al., 2005). During the period of low sea level, terrigenous sediments transported by the Han River, Pearl River, Red River and intermountain rivers of the Indo-China Peninsula directly crossed the exposed continental shelf and entered the basin, promoting the development of the submarine channel/canyon systems. The South Taiwan Bank Canyon corresponding to the Han River was formed at ~13.8 Ma in the Middle Miocene (Ding et al., 2010); and the Pearl River Canyon connected to the Pearl River also continued to be active during

this period (Ding et al., 2013; Chen et al., 2020). These canyon systems became the main conduits for the transport of terrigenous materials, and depositional centers were developed at the mouth (Fig. 4C). Compared to the northern slope foot area of the oceanic basin, the sedimentation in the center was still limited. Sites U1433 and U1431 near the fossil spreading ridge of the SWSB and ESB, encountered ~50 m and ~200 m sediment of this period. Based on Sr-Nd isotopic analysis on the Site U1431, Liu et al. (2021) concluded that the sedimentary provenance since ~12.8 Ma was mainly from the Pearl River system, indicating that the terrigenous sediments in the Middle Miocene still dispersed from the northern flank of the SCS to the center.

Although the sediment budget in the SWSB had increased significantly during the Middle Miocene ($4.23 \times 10^3 \text{ km}^3/\text{my}$), it was much lower than that of the Mekong shelf ($31.0 \times 10^3 \text{ km}^3/\text{my}$) and the slope region ($25.7 \times 10^3 \text{ km}^3/\text{my}$) (Fig. 6). Previous studies indicated that the southern continental margin experienced a westward propagated rifting. The unconformity marking the rifting cessation is diachronous and gets younger from east to west (Li and Song, 2012; Savva et al., 2014; Franke et al., 2014; Ding et al., 2016). The transport sequence of terrigenous sediments via rivers is shelf-slope-oceanic basin. During the Middle Miocene, the rifting in the Mekong shelf area was still active and continued to the Late Miocene, producing enough space to accommodate sediment, and the sediment budget on the Mekong shelf reached its peak (Fig. 6). Although the sediment budget increased in the southwest slope area of the SCS (including the Mekong slope area, Zhongjia Basin and Nansha Islands) (Fig. 6), it was not as obvious as that in the Mekong shelf area. Although the sediment budget is relatively low in the SWSB, the sediments that entered the SWSB still formed a depocenter in the southwest corner (Fig. 4C). In the southern flank of the ESB, the limited depocenter, mainly at the slope foot in the southeast, is associated with the terrigenous sediments input through the Northern Palawan Canyon formed at ~15 Ma (Yin et al., 2018).

5.1.4. Late Miocene (11.6 Ma - 5.3 Ma)

In the Late Miocene, the sediment budgets of continental margin basins showed a significant decrease, except for the southwest slope area of the SCS (including the Mekong slope area, Zhongjia Basin and Nansha area) (Fig. 6). Clift (2006) suggested that the decrease in the rate of land-based denudation rate during the Late Miocene might be related to the prevailing Asian winter monsoon and arid climate. The chemical weathering history reconstructed by the chemical alteration index of Site ODP 1148 in the northern continental margin of the SCS also showed that the humidity in South China began to decrease since the Late Miocene (Wang et al., 2003; Wan et al., 2007). The cold and dry climate weakened the land denudation, and the sediments transported via onshore rivers decreased, resulting in low sediment budget in the continental shelf (Wan et al., 2006, 2007).

Different from the continental margin, the sediment budgets in SCS oceanic basins further increased (with an increment of $4.40 \times 10^3 \text{ km}^3/\text{my}$), and reached the peak in the NWSB ($2.61 \times 10^3 \text{ km}^3/\text{my}$) (Fig. 6). Either the thickness or distribution range of sediments increased sharply (Fig. 4D). This opposite trend between the SCS oceanic basin and continental margin may be related to superposition of three factors: (1) the Central Canyon began to develop at ~11.6 Ma (Su et al., 2016, 2014; Shao et al., 2019; Chen et al., 2020), providing a transport channel for the sediments carried by the Red River and the small mountain rivers of the eastern Indo-China Peninsula to enter the NWSB; (2) An anomalous rapid subsidence occurred in the Baiyun Sag during the Middle Miocene (Fang et al., 2022), providing accumulation space for sediments. However since the Late Miocene, the subsidence rate and the sedimentation rate in the Baiyun Sag reduced remarkably in the Baiyun Sag (Xie et al., 2013). The terrestrial sediments carried by the onshore river systems would have flowed over the shelf area and mainly deposited in the continental slope and abyssal basin. Multiple regressions during this stage also favored the direct transportation of the terrigenous sediment into the abyssal basin through channel/canyon systems (Pang et al.,

2005), such as the Central Canyon, Pearl River Canyon, and South Taiwan Bank Canyon, etc. As shown in Fig. 4D, the three depocenters in the northern SCS not only had a significant increase in thickness, but also overlapped with each other in their distribution ranges; (3) The uplift event in the Dongsha Islands, which lasted from 13.8 Ma to 2 Ma and was most active at ~5.5 Ma. It is generally accepted that this event was caused by magma intrusion into the basement (Lüdmann and Wong, 1999; Sun et al., 2014). The absence of Neogene strata at the top of the Dongsha Islands demonstrated that the area has experienced intense erosion (Luan et al., 2012). Denuded sediments may eventually be transported to the northern part of the SCS oceanic basin (Ma and Tian, 2015; He et al., 2017), forming the depocenter at the slope foot of the Dongsha Islands.

Unlike the ESB and NWSB, the sediment budget in the SWSB reduced slightly during the Late Miocene (decreased by $0.35 \times 10^3 \text{ km}^3/\text{my}$) (Fig. 6), which might be related to sediment capture in the Mekong slope area. During this period, the rifting in the Mekong Shelf ceased, the rifted basins were filled, and terrigenous sediments began to accumulate across the shelf to slope, resulting in the rapid increase of sediment budget (with an increment of $\sim 20 \times 10^3 \text{ km}^3/\text{my}$) in the southwest slope area of the SCS, such as the Mekong slope area, the Zhongjia Basin and Nansha Islands (Fig. 6). Meanwhile, based on seismic profiles' interpretations, Li et al. (2012) implied that the rifting continued until the Early Pliocene (~5.3 Ma) in the Mekong slope area, thus there was still space to accommodate sediments, leading to the relative reduction of sediment budget in the SWSB. Although the overall sediment budget decreased, both the thickness and distribution range of the depocenter in the southern flank of the ESB and the southwestern SWSB increased compared with those in the Middle Miocene, and gradually dispersed towards the center of the basin (Fig. 4C and D). The former was located in the mouth of the North Palawan Canyon, while the latter was related to the Penxi Canyon in the southeast of the Zhongjia Basin (Zhu et al., 2017; Luo et al., 2018), as well as the Mekong River Abyssal Channels in the southwest corner of the SWSB (Guan et al., 2016), which were both formed in the Late Miocene. According to the sediment isotope analysis of Site U1433 (Liu et al., 2017b), the modern Mekong River gradually became the major sediments supply of the SWSB since ~8 Ma.

5.1.5. Pliocene (5.3 Ma - 1.8 Ma)

Since the Pliocene, the distribution pattern of sediments in the SCS oceanic basin had changed, i.e. either the range or thickness of the depocenters at the slope foot area in the NWSB and the northern flank of the ESB decreased, but in the southern flank of the ESB and the entire SWSB increased substantially with an average thickness between 150 m and 200 m, except for basement highs or seamount chains along the relic spreading ridge (Fig. 4E). During this period, the East Asian summer monsoon prevailed again, and the climate changed to warm and humid (Wan et al., 2006; Clift et al., 2014), which intensified the denudation on land, and promoted the sediment transportation into the ocean via the river systems. However, due to the high sea level at the Pliocene (Fig. 5; Pang et al., 2005), the broad shelf of the northern SCS (>350 km) had a huge accommodation space. Terrigenous sediments transported via the onland river systems, including the Red River, Pearl River, Han River, and alpine rivers in Taiwan Island, might preferentially accumulate in the estuarine shelf area, causing the increased sediment budgets in the Yinggehai Basin, Qiongdongnan Basin, Pearl River Mouth Basin, and Taixinan Basin (Fig. 6). However, the submarine canyon systems in the northern continental margin generally retreated in the Late Pliocene. The distribution of the Central Canyon was limited to the east of the Qiongdongnan Basin due to changes in the tectonic-sedimentary environment during 3.8 Ma – 1.8 Ma (Su et al., 2014; Chen et al., 2020); the transporation capacity of the Pearl River Canyon was also greatly reduced, and the sediment was mainly accumulated in the channels (Ding et al., 2013). Therefore, the sediment budget of the NWSB decreased, and either the sedimentary thickness and range in the

northern flank of the ESB decreased significantly compared with those in the Late Miocene (Fig. 4E). According to the drilling results of the Site U1499 in the north, the Pliocene sediment is mainly composed of deep-sea mudstone with a thickness of ~200 m, which was significantly thinner than the Upper Miocene with a thickness of nearly 530 m (Fig. 2; Sun et al., 2018). The only remarkable depocenter in the northern flank was located at the slope foot near the Dongsha Islands, which was presumed to be related to the continuous uplifting of the Dongsha Islands (Fig. 4E). The Taiwan Island orogeny started at in the Late Miocene, feeding eroded sediments from ongoing tectonic uplift into the SCS (Dadson et al., 2003; Milliman and Farnsworth, 2011). However, due to the fact that Taiwan Island located further eastward compared to the present location during the Pliocene, most of the deposition have been subducted beneath the Maria Trench, although parts of them could reach the central basin even to Site U1431. Based on the analysis of the heavy minerals and detrital zircon maps on the sediments of the Site U1431 (Cao et al., 2021; Liu et al., 2021), during this stage the sediments in the center oceanic basin were mainly originated from the Indo-China Peninsula in the west, with some contribution from the Pearl River and Red River.

It is worth noting that under the condition of uniform East Asian monsoon event and sea level change, the sediment budget curve shows an opposite increasing trend in the SWSB (with an increment of $2.97 \times 10^3 \text{ km}^3/\text{my}$) Compared with the north, the western continental shelf of SWSB is much narrower (no more than 150 km), which responded more rapidly to the denudation caused by regional tectonic events, or to the monsoon and sea level changes. The route of sediments transported by the Mekong River from land and sea was much shorter than that of the Pearl River or the Red River in the northern during a high sea level period. As the rifted basins of the Mekong Slope area were filled up in the Pliocene (Li et al., 2012; Franke et al., 2014; Ding et al., 2016), terrigenous sediments began to be transported across the slope to the deep ocean, which is indicated by the decreased sediment budget in the western slope area (including the Mekong slope area, Zhongjiaannan Basin and Nansha area), and the increased one in the SWSB (Fig. 6). Either the thickness or range of the depocenters increased significantly compared with the Late Miocene (Fig. 4E). Drilling results of the Site U1433 show that the sediment thickness in this period reached ~200 m, and the lithology was dominated by deep-sea clay interbedded with carbonate deposits (Li et al., 2015b). Combined with isotopic analysis of the sediments in this site (Liu et al., 2017b), we suggest that the sediments were still mainly from the modern Mekong River, with some contribution from the carbonate platform in the Nansha Islands (Ding et al., 2013).

The sediment budget in the ESB increased slightly (with an increment of $1.54 \times 10^3 \text{ km}^3/\text{my}$), which were mainly due to the contribution of the southern flank. The depocenter lying in the mouth of North Palawan Canyon had a larger depocenters either in range or thickness (Fig. 4E), suggesting the major contribution from the Palawan. (Fig. 6).

5.1.6. Pleistocene - present (1.8 Ma- 0 Ma)

Since the Pleistocene, the sediment budgets increased in each subbasins (with an increment of $21.94 \times 10^3 \text{ km}^3/\text{my}$ for the whole oceanic basin), although the magnitude was not consistent. The sedimentary accumulation mainly focused on the SWSB and the northeast part of the ESB (Fig. 4F). The sediment thickness of Site U1433 in the SWSB reaches to ~330 m in this stage, which is much higher than the ~210 m of Site U1499 in the NWSB, or the ~130 m of Site U1431 near the fossil spreading ridge of the ESB (Fig. 2). The sediment budget increased slightly (with an increment of $0.86 \times 10^3 \text{ km}^3/\text{my}$) in the NWSB, with no obvious depocenter. The deposits were mainly distributed at the mouth of the Central Canyon, which might be related to the Central Canyon's rejuvenation after the Pleistocene with the increase of sediment recharge capacity due to climate change (Chen et al., 2020; Su et al., 2014, 2016). Although the sediments at the mouth of the Pearl River Canyon and the slope foot of the Dongsha Islands retreat further,

there developed a significant depocenter with large thickness and wide range at the low reach of the channel and canyon systems offshore Taiwan Islands (Fig. 4F). Both ODP sites 1146 and 1148 proved that the terrigenous mass accumulation rate (MAR) has increased by 2–14 times since ~ 3 Ma (Wan et al., 2010). Meanwhile, the thickness of the sediments in the southern ESB is further enlarged, and the depocenters are mainly concentrated at the mouth of the North Palawan Canyon, as well as the southeastern corner of the oceanic basin (Fig. 4F). During this stage, the sediments of the Site U1431 in the central of the ESB are mainly composed of deep-sea clay embedded with silts and siltstones with thickness ranging from meters to tens of meters, indicating episodic turbidite events (Li et al., 2015b). The geochemical analysis showed that the sediments were originated from the Pearl River and Taiwan Island (Cao et al., 2021; Liu et al., 2021). The budget of the SWSB also increased significantly (with an increment of $16.52 \times 10^3 \text{ km}^3/\text{my}$), and the deposition centers were mainly concentrated on the mouth area of the submarine channel/canyon systems developed in the southern continental margin, including the Penxi Canyon and the Mekong River Abyssal Channels in the southwest corner, and dispersed to the center (Fig. 4F). A large set of deep-sea facies clay were developed in Site U1433 in the SWSB, which were mainly contributed by the modern Mekong River (Liu et al., 2017b).

The intensification of the interglacial summer monsoon and the frequent glacial-interglacial climate change are consistent with the rapid increase in sediment budgets since the Pleistocene, which is also consistent with the increasing $\delta^{18}\text{O}$ curve (Fig. 5). This rapid changes in sedimentation rates can be observed in many other areas either on land or in the ocean including the Alpine in Europe (Kuhlemann et al., 2002), the Angola Continental Margin in West Africa (Lavier et al., 2001), and the offshore part of the Amazon Basin (Figueiredo et al., 2009), etc. confirmed that the increase in sediment budget is a global phenomenon. Zhang et al. (2001) suggested that this phenomenon was driven by frequent changes caused by global climate deterioration. Meanwhile, as the global sea level has declined since the Pleistocene (Haq et al., 1987), climate factors and sea-level influences lead to a rapid increased in terrigenous sediments entering the SCS oceanic basin through submarine canyon/channel systems (Ding et al., 2013; Su et al., 2014, 2016). Sediments are concentrated at the mouth area of submarine canyon/-channel systems, such as the Penghu-Kaoping Canyon, the Pearl River Canyon, the Central Canyon, the Penxi Canyon, the Mekong River Abyssal Channels, and the North Palawan Canyon, especially the huge depocenter along the Manila Trench in the NE part of the oceanic basin (Fig. 4F). The continuous uplift of Taiwan Island resulted in great weathering and denudation, with the erosion rate estimates range from 2.2 to 8.3 mm/yr for records with varying sampling frequencies and durations between 8 and 27 yr (Fuller et al., 2003). Seasonal inter-mountain river runoff is extremely high in southwestern Taiwan Island. In present the sediment loads from the Cho-Shui River and the Kao-Ping River can reach to 54.1 Mt/yr and 49 Mt/yr, respectively, which are largest in Taiwan Island (Liu et al., 2016). Huge amounts of terrigenous sediments carried by rivers have entered into the abyssal basin via amounts of channel/canyon systems developed in the southwest slope area offshore Taiwan Island, forming a huge submarine accumulation fan (>1000 m) expanding to the abyssal basin (Fig. 4F).

5.2. Sedimentary provenance

The sediments in the SCS oceanic basin mainly include volcanic deposits such as basalt, biogenic carbonate deposits, and deep-sea claystone, siltstone, sandstone deposits (Li et al., 2015b; Sun et al., 2018). Volcanic deposits are mainly distributed around seamount or seamount chains in the abyssal basin, with a narrow range and small volume, which was not considered in this paper. Carbonate deposits are mainly distributed around the Zhongsha, Xishan and Nansha Islands (Gong et al., 2005; Wu et al., 2014; Shao et al., 2017; Huang et al., 2020), and the terrigenous sediments mainly come from large land river

systems (such as the Pearl River, the Red River, and the Mekong River) and alpine rivers (such as the Gaoping River in southwestern Taiwan and the intermountain rivers in the eastern Indo-China Peninsula) (Liu et al., 2016). In this study, based on the calculation results of sediment budgets in the SCS oceanic basin and the sedimentary isopach maps, the drilling result and the analysis of previous geochemical work of the IODP and ODP sites, as well as the evolution of the major river/canyon/channel systems and tectonic events, the possible sedimentary provenances of the NWSB, the SWSB and the ESB in different geological time were analyzed.

5.2.1. Sedimentary provenance of NWSB

According to the location of the NWSB, the Pearl River in the north and the Red River in the northwest were likely to control the sedimentary transport process in the NWSB and its adjacent areas. In addition, Hainan Island in the northwest, Zhongsha and Xisha Islands in the south, and local basement uplifts in the shelf area might also be the provenances.

During the Oligocene (33 Ma - 23 Ma), the sediments in the NWSB mainly came from the surrounding basement highs, such as the Zhongsha Islands and the Reed Bank (Fig. 4A). The Pearl River system would have also made some contribution (Ma et al., 2019; Liu et al., 2022). In the Early Miocene (23 Ma - 16 Ma), the further development of the Pearl River incised the slope area in the north, leading to the formation of Pearl River Canyon system (Ding et al., 2013; Cao et al., 2018). Geochemical analysis on Site U1435 and industrial wells in the north of SCS showed that the Pearl River and its tributaries were the main sedimentary provenance of the northern margin (Liu et al., 2017a). Therefore, the NWSB terrigenous sediments mainly came from the northern Pearl River and were transported through the Pearl River Canyon (Fig. 4B). At this time, the Central Canyon was not developed, and the sediments from the central Vietnam and Hainan Island were mainly limited in the Qiongdongnan Basin, but rarely entered the NWSB (Yao et al., 2008; Zhao et al., 2015). During the Middle Miocene (16 Ma - 11.6 Ma), the seafloor spreading of the SCS ceased, and the sedimentary supply of the NWSB was basically consistent with that of the Early Miocene (Fig. 4C). The Pearl River was once a small river confined to the coast of South China during the Early Oligocene, and came into the present pattern during the Middle Miocene (Cao et al., 2018). The sediment budgets in the Pearl River Mouth Basin and Baiyun Sag were much higher than that in the Qiongdongnan Basin (Fig. 6), indicating that the sediments of NWSB mainly came from the Pearl River in the north, rather than the Red River in the west.

During the Late Miocene (11.6–5.3 Ma), the East Asia was dominated by the winter monsoon (Wan et al., 2007; Holbourn et al., 2018), and the climate became cold and arid, resulting in weakened denudation of the South China and the Indo-China Peninsula. However, uplift events caused by the eruption of magmatic rocks occurred in Vietnam (~8 Ma) and Dongsha (~5.5 Ma) in the Late Miocene, leading increased weathering and denudation (Ma et al., 2015; He et al., 2017). During the low sea level period the canyon/channel could directly transport terrigenous sediments into the NWSB, such as the still active Pearl River Canyon (Ding et al., 2013) and the Central Canyon formed in the Late Miocene (Su et al., 2014, 2016). However, the low sedimentary budget either in the Yinggehai basin or Qiongdongnan Basin indicated that the sedimentary contributions of the Central Canyon system to the NWSB were still limited.

During the Pliocene (5.3 Ma - 1.8 Ma), due to the relatively high sea level of the SCS (Pang et al., 2005), both the Central Canyon and the Pearl River Canyon retreated (Fig. 4E), and most of the sediments accumulated on the shelf area. Based on the low-temperature thermochronology research, Shi et al. (2011) described the Cenozoic erosion history in southern Hainan Island, suggesting that the supply of terrigenous sediments might have increased since ~ 5 Ma. Zhu et al. (2008) further demonstrated that within 4.2 Ma - 3.7 Ma, a submarine fan-shaped delta developed in the southern part of Hainan Island,

providing provenance evidence for the NWSB. In the slope area near the Yitong-Ansha Uplift in the north of the NWSB, large sets of mass transport deposits (MTDs) were developed by transporting terrigenous detrital materials in gravity flow through the slope area into the NWSB in a short time since the Pliocene (Wu et al., 2011), and the MTDs were also found in the Central Canyon on the west side of the NWSB during the same period (Shang et al., 2015; Chen et al., 2020).

Since the Pleistocene (1.8 Ma - 0 Ma), the sediments could transported into the deep NWSB through the Pearl River Canyon and the rejuvenated Central Canyon during the episodic low sea level period, resulting in the two sedimentary belts close to the canyon mouths in Fig. 4F. Possible sediment provenances include the Pearl River in the north, the Red River in the west, the Hainan Island, small mountain rivers in eastern Indo-China Peninsula, and even the suspended sediments from Taiwan Island by ocean currents. (Liu et al., 2016).

Carbonate deposits, including carbonate platforms and coral reefs on top of basement uplifts, developed extensively in the Xisha and Zhongsha Islands since the Late Oligocene (Ma et al., 2011). However, in the NWSB, the sediments are mainly composed of ultramicrofossil rich shale, silty interlayer shale, clay, silty sandstone and silt (U1499, U1500, and U1502, Sun et al., 2018; Jian et al., 2018). Biogenic carbonate content was basically <0.5 wt% (Sun et al., 2018), since most carbonate deposits have been drownsince the Middle Miocene (Ding et al., 2013; Ma et al., 2011). The contribution of carbonate was very limited.

5.2.2. Sedimentary provenance of ESB

Since the seafloor spreading of the ESB began in the Oligocene, the Pearl River and the Han River had controlled the transport and deposition processes on the northern SCS. In addition, The Palawan in the south, and local basement highs such as the Reed Bank might also transport sediments to the oceanic basin. Based on the geochemical analysis of Site ODP1148 on the north SCS, Wei et al. (2012) believed that since the SCS was still a long and narrow bay before ~26 Ma, sediments from the Palawan could be transported to the north side of the SCS.

The Pearl River and the Han River were the two major supply sources of terrigenous materials in the northern part of the SCS since the Paleogene. In the Oligocene (33 Ma - 23 Ma), compared with the Pearl River which was still in its development stage, the pattern of the Han River has basically been formed (Zhang et al., 2012, Fig. 4A). Distribution characteristics and discriminant analysis of rare earth elements showed that, during the Early Miocene (23 Ma - 16 Ma), the distribution range of the Han River was further expanded, which corresponded to the significant depocenter in the ESB of Fig. 4B. Similar to the NWSB, the northern flank of the ESB also received terrigenous sediments from the Pearl River transported through the Pearl River Canyon.

During the Middle Miocene (16 Ma - 11.6 Ma), the Han River gradually retreated, and based on the single-grain zircon provenance methods, the Pearl River evolved from a small river confined to the coast of the South China during the Early Oligocene, and gradually developed into the modern pattern in the Middle Miocene (Liu et al., 2017a; Cao et al., 2018). Since then, it has replaced the Han River as the main sedimentary provenance in the northern margin of the SCS (Zhang et al., 2012). In addition, in the southern ESB, sediments were also accumulated at the slope foot of the ESB through the Northern Palawan Canyon formed at ~15 Ma (Fig. 4C), indicating the contribution from Palawan.

In the Late Miocene (11.6 Ma - 5.3 Ma), due to the prevailing winter monsoon, cold and arid climate resulted in weakened denudation in South China, and reduced the transportation capacity of the Han River and Pearl River (Fig. 4D). In this period, the terrigenous sediments from the Pearl River and the Han River were input to the north flank of the ESB through the Pearl River Canyon and the Taiwan Bank Canyon, respectively, and the denudation of local structural uplift (Dongsha Islands uplift event) would also contributed the sediments. The sediment source analysis of Site U1431 in the center of the ESB showed that sediments mainly came from the Pearl River system. In addition, due to

the uplift event in Vietnam, some sediments from the eastern Indo-China Peninsula were also transported to the abyssal plain (Cao et al., 2021).

During the Pliocene (5.3 Ma - 1.8 Ma), the SCS was in a period of high sea level, and the northern ESB was dominated by the sediments from the Pearl River system and the denuded sediments from the Dongsha Islands. Meanwhile, the Taiwan orogeny promoted the transportation of terrigenous materials produced by the uplift and denudation into the oceanic basin via the alpine rivers of Taiwan Island, and gradually became the major sedimentary provenance of the ESB after ~3 Ma (Wan et al., 2010; Liu et al., 2021). Based on the analysis of siliciclastic turbidite in Site U1431, Cao et al. (2021) suggested that the Indo-China Peninsula in the west was also the sedimentary provenance of the central basin during the Pliocene.

Since the Pleistocene (1.8 Ma - 0 Ma), the Dongsha- South Taiwan Bank - Penghu- Kaoping Canyon System in the northeast of the oceanic basin gradually formed, and the mountain rivers from the southwest of Taiwan Island gradually became one of the main provenances. A huge amount of sediments accumulated along the Manila Trench in the northeast, forming a abyssal fan-shaped deposits with a thickness of more than 1000 m (Fig. 4F). The Manila Trench and the Luzon arc captured most of the terrigenous sediments originating from the Luzon Islands, but some of them still entered the ESB near the Manila Trench, especially in the southeast corner of the SCS.

5.2.3. Sedimentary provenance of SWSB

Considering the natural geographical conditions of the SWSB, there were many possibilities for the sedimentary provenance, such as the Borneo in the south, the Sunda shelf in the southwest, and the Indo-China Peninsula in the west. The Borneo in the south collided with the Nansha Islands at ~16 Ma, but the uplift and denudation at the northern tip were weaker (Honza et al., 2000). Furthermore, the Borneo was separated from the SCS oceanic basin by the board Nansha Islands with well-developed faulted sags and blocks, favoring sediments accumulation (Ding et al., 2013). Therefore, most of the sediments from the Borneo were deposited in the Nansha Islands, which was consistent with the large sediment budget (Fig. 6), and the Borneo might not be the major provenance of the SWSB. Only during the period of low sea level (such as Middle Miocene and the Pleistocene to present) could sediments from the Sunda shelf and Malay peninsula have crossed the exposed the Sunda shelf into the SWSB via the Molengraaff river (Clift, 2006; Liu et al., 2016). Similarly, the Red River and the Pearl River in the north were far away from the SWSB, and the sediments transported by the Red River were mainly accumulated in the Yinggehai Basin. The Pearl River Mouth basin has experienced rapid a thermal subsidence since the Middle Miocene (Chen, 2014; Clift et al., 2015), and could accommodated the sediments transported by the Pearl River. Therefore, during the Early Miocene (23 Ma - 16 Ma), the sediments of the SWSB were mainly contributed by the local basement highs (such as the Reed Bank) (Fig. 4B).

During the Middle Miocene (16 Ma - 11.6 Ma), the sediments of Site U1433 in the SWSB are featured with high $^{87}\text{Sr}/^{86}\text{Sr}$ and negative Nd anomaly, which is similar with that of the small mountain rivers in the Indo-China Peninsula (Liu et al., 2016b; Jonell et al., 2017). Moreover, the Indo-China Peninsula has a narrow shelf, so the eastern Indo-China Peninsula were the most likely sediment provenance of SWSB during this stage (Fig. 4C). This is also consistent with the previous statement that the acceleration of sediment budget in SWSB during this period was attributed to the uplift of the Tibet Plateau and the enhancement of denudation caused by the acceleration of extrusion of relevant blocks (including Indo-China blocks) in the southeast (Clark et al., 2005). In addition, the Palawan, which is closer to the SWSB, could also provide contribution.

The drilling results showed that the Late Miocene lithology of Site U1433 was dark green to gray green claystone embedded with thick gray green ultrafossil carbonate (Fig. 2; Lei et al., 2015). Ding et al. (2016) analyzed the sedimentation rates in different areas of the SWSB, and

results showed that the rate in the southwest of the oceanic basin were higher than that in the northeast during the Late Miocene (11.6 Ma - 5.3 Ma), indicating that the sediments mainly came from the southwest direction. Studies on the northern margin of the SCS suggested that chemical weathering intensity had been decreasing since ~16 Ma (Clift et al., 2014), and the increase of sediment budgets in the SWSB since the late Miocene might indicate that sediments were imported from the Mekong River and some small mountain rivers in the Indo-China Peninsula under stable climatic conditions (Fig. 4D). Based on multi-beam and seismic data, Guan et al. (2016) discovered multiple buried abyssal channels developed during the Late Miocene in the southwestern slope of the SCS, which acted as important pathways for conveying terrigenous materials to the SWSB through the shelf, indicating that the SWSB was contributed by terrigenous sediments from the Indo-China Peninsula. In addition, Nd and Sr isotopic evidence showed that the sediments from Site U1433 were similar to the modern Mekong River, which further indicated the contribution of the Mekong River System since ~8 Ma (Liu et al., 2017b).

During the Pliocene (5.3 Ma - 1.8 Ma), the main sedimentary provenance of the SWSB was from the Indo-China Peninsula, especially via the modern Mekong River (Fig. 4E). Since the Pleistocene (1.8–0 Ma). There were also contributions from the Sunda shelf and the Malay Peninsula during low sea level period (Fig. 4F).

Since the Late Oligocene, carbonate deposits, including carbonate platforms and reefs formed in tectonic highlands, were widely developed in both the southern and northern continental margin basins of the SCS (Wu et al., 2011; Ma et al., 2011; Xie et al., 2020). Although most of the carbonate platforms were drowned since the Middle Miocene, reefs formed on baement highs could grow until the late Miocene (Steuer et al., 2014). The transport of the widely developed carbonate deposits to the oceanic basin resulted in the formation of chalk with thickness exceeding 1 m in the SCS oceanic basin. Since the Pliocene, drilling results showed that carbonate deposits suddenly became thinner and disappeared after the Early Pleistocene, which was related to the increased tectonic subsidence in the margin of the SCS and the rise of sea level. Only in some areas, such as Reed Bank, Zhongsha Islands and Nansha Islands, the corel reefs have grown up to present, but their contribution to carbonate deposition in abyssal basin was very small.

6. Conclusion

Based on more than 30 multichannel seismic profiles covering the whole oceanic basin, combined with the drilling results from the IODP 349, 367 & 368 Expeditions in the SCS as constraints, we calculated the sediment budget of the whole oceanic basin of the SCS, characterized the million-year-timescale quantification of sediment dispersal and accumulation process of the SCS oceanic basin, and discussed the relationship to the region and local tectonic events, Asian monsoon, sea level changes, submarine channel/canyon system developments, etc., aiming to document the mechanisms controlling the spatio-temporal sediment budget variation, as well as the possible sedimentary provenance.. The conclusions are as follows:

1. During the Oligocene (33 Ma - 23 Ma), the SCS began to open, and the sediment budget was in a small scale ($4.38 \times 10^3 \text{ km}^3/\text{my}$). The local depocenters were generally close to the basement highs in the continental shelf, which is speculated to be related to the weathering and denudation of the tectonic highs. During the Early Miocene (23 Ma - 16 Ma), there were two local depocenters locating in the lower reaches of the Han River delta in the northeast and at the mouth of the Pearl River Canyon system. The sediment thickness gradually thinned from ocean basin margin to the spreading ridge. During the Middle Miocene (16 Ma - 11.6 Ma), the terrigenous sediments mainly accumulated in the northern flank of the basin, and the sediment budget increased rapidly to $13.50 \times 10^3 \text{ km}^3/\text{my}$ due to the uplifting event of the Tibet Plateau and intensification of the East Asian

- summer monsoon. In the Late Miocene (11.6 Ma - 5.3 Ma), the sediment budgets in SCS oceanic basin increased to 17.90×10^3 km³/my. The increase of either the sediment thickness or distribution range may be related to the formation of the Central Canyon in the west, the active Pearl River Canyon in the north, episodic sea level drops, and local uplift events (i.e. Dongsha Islands, central Vietnamese plateau). During the Pliocene (5.3 Ma - 1.8 Ma), the East Asian summer monsoon prevailed again, and the climate changed to warm and humid, which intensified the denudation on land. The sediment budget of the SCS oceanic basin continued to increase to 21.32×10^3 km³/my. Since the Pleistocene, the sediment budgets suddenly increased to 60.64×10^3 km³/my, nearly three times as before. This rapid increasing in sediment budgets can be observed in most the continental margin basins of the SCS at the same time. The intensification of the interglacial summer monsoon and the frequent glacial-interglacial climate change are consistent with the rapid increase in sediment budgets since the Pleistocene, which is also consistent with the increasing $\delta^{18}\text{O}$ curve.
2. Sediment budget decrease event occurred in the SWSB during the Late Miocene, and in the NWSB during the Pliocene. The former might be related to the sedimentary capture in the Mekong slope area. The continental rifting was still active during this period, and most of the terrigenous sediments were deposited in the slope area rather than entering into the abyssal basin. The decrease of sediment budgets in the NWSB during the Pliocene was mainly related to the high sea level and the retreated of the Central Canyon.
3. During the Pliocene (5.3 Ma - 1.8 Ma), the distribution pattern of sediments in the SCS oceanic basin had changed significantly. Before then, the sediments accumulation main focused on the northern flank, with the depocenters generally distribute at the mouth of the submarine channel/canyon systems and slope foot area near basement highs; but gradually migrated to the southern flank since the Pliocene due to the high sea level and the increase of Mekong River runoff. An exception is the depocenter in the northeast part related with the Taiwan orogeny, forming a huge submarine accumulation fan (>1000 m) expanding to the central basin.
4. The sediment sources of different sub-basins in the SCS changed gradually over time. Since the opening of the ESB and NWSB in the Oligocene, the Pearl River and the Han River had controlled the accumulate and disperse processes on the northern SCS. During the Middle Miocene (16 Ma - 11.6 Ma), the Pearl River gradually developed into the modern pattern and became the major sedimentary provenance in the northern margin of the SCS. Local tectonic events, including the Dongsha event and the uplift of central Vietnamese plateau during the Late Miocene, and the uplift of the Hainan Island during ~5 Ma, also might contribute to the sedimentation supply of the NWSB and the northern flank of the ESB since the Late Miocene. During the Pliocene (5.3 Ma - 1.8 Ma), the northern ESB was dominated by the sediments from the Pearl River system and the denuded sediments from the Dongsha Islands. Taiwan Island became the sedimentary provenance of the northern ESB after ~3 Ma. The sediments of the southern ESB mainly originated from North Palawan area. The terrigenous sediment sources of the SWSB changed a lot at ~ 8 Ma. Before that, the sediment source included the intermontane rivers of the Indo-China Peninsula and small contributions from the North Palawan, while after that the sediments mainly came from the modern Mekong River.

Declaration of competing interest

The authors declare that they have no known competing financial interests or personal relationships that could have appeared to influence the work reported in this paper.

Data availability

Data will be made available on request.

Acknowledgments

We appreciated the constructive discussion with Xinong Xie, Rong Yang and Sean Willett. We are grateful to the IODP China Office, the JOIDES Resolution drilling vessel technical staff and crew for their contributions during sample collection during the International Ocean Discovery Program (IODP) 349, 367 & 368 Expedition. The paper was improved following comments from Qiliang Sun and two anonymous reviewers. All the drilling data can be accessed via the web address (<http://iodp.tamu.edu/publications/proceedings.html>). The scientific graphics software, Suffer was used to make sedimentary isopach maps in this work. This work was funded by the National Natural Science Foundation of China (Grant Nos. 42025601, 91858214), and the Leading Talents in Scientific and Technological Innovation Project of Zhejiang Province (No. 2019R52034).

References

- Barckhausen, U., Engels, M., Franke, D., Ladage, S., Pubellier, M., 2014. Evolution of the South China Sea: revised ages for breakup and seafloor spreading. *Mar. Petrol. Geol.* 58, 599–611. <https://doi.org/10.1016/j.marpetgeo.2014.02.022>.
- Briais, A., Patriat, P., Tappisonnier, P., 1993. Updated interpretation of magnetic anomalies and seafloor spreading stages in the south China Sea: implications for the Tertiary tectonics of Southeast Asia. *J. Geophys. Res. Solid Earth* 98 (B4), 6299–6328. <https://doi.org/10.1029/92JB02280>.
- Cameselle, A.L., Ranero, C.R., Franke, D., Barckhausen, U., 2017. The continent-ocean transition on the northwestern South China Sea. *Basin Res.* 29, 73–95. <https://doi.org/10.1111/bre.12137>.
- Cao, L., Shao, L., Qiao, P., Zhao, Z., van Hinsbergen, D.J.J., 2018. Early Miocene birth of modern Pearl River recorded low-relief, high-elevation surface formation of SE Tibetan Plateau. *Earth Planet Sci. Lett.* 496, 120–131. <https://doi.org/10.1016/j.epsl.2018.05.039>.
- Cao, L., Jiang, T., He, J., 2021. Fingerprinting sand from asian rivers to the deep central south China sea since the late Miocene. *GSA Bulletin* 133 (9–10), 1964–1978. <https://doi.org/10.1130/B35845.1>.
- Caracciolo, L., 2020. Sediment generation and sediment routing systems from a quantitative provenance analysis perspective: review, application and future development. *Earth Sci. Rev.* 209, 103226 <https://doi.org/10.1016/j.earscirev.2020.103226>.
- Carter, A., Roques, D., Bristow, C.S., 2000. Denudation history of onshore central Vietnam: constraints on the Cenozoic evolution of the western margin of the South China Sea. *Tectonophysics* 322 (3–4), 265–277. [https://doi.org/10.1016/S0040-1951\(00\)00091-3](https://doi.org/10.1016/S0040-1951(00)00091-3).
- Chen, L., 2014. Stretching factor estimation for the long-duration and multi-stage continental extensional tectonics: application to the Baiyun Sag in the northern margin of the South China Sea. *Tectonophysics* 611, 167–180. <https://doi.org/10.1016/j.tecto.2013.11.026>.
- Chen, H., Xie, X., Mao, K., He, Y., Su, M., Zhang, W., 2020. Depositional characteristics and formation mechanisms of deep-water canyon systems along the northern south China sea margin. *J. Earth Sci.* 31 (4), 808–819. <https://doi.org/10.1007/s12583-020-1284-z>.
- Chen, H., Stow, D.A., Xie, X., Ren, J., Mao, K., Gao, Y., et al., 2021. Depositional architecture and evolution of basin-floor fan systems since the late Miocene in the northwest sub-basin, south China sea. *Mar. Petrol. Geol.* 126, 104803.
- Chen, Y., Yan, M., Fang, X., Song, C., Zhang, W., Zan, J., Zhang, D., 2017. Detrital zircon U-Pb geochronological and sedimentological study of the Simao Basin, Yunnan: Implications for the Early Cenozoic evolution of the Red River. *Earth Planet Sci. Lett.* 476, 22–33.
- Chiang, C.-S., Hsiung, K.-H., Yu, H.-S., Chen, S.-C., 2020. Three types of modern submarine canyons on the tectonically active continental margin offshore southwestern Taiwan. *Mar. Geophys. Res.* 41 (1), 4. <https://doi.org/10.1007/s11001-020-09403-z>.
- Chuang, C., Yu, H., 2002. MorPhology and canyon forming processes of upper reach of the Penghu submarine canyon off southwestern taiwan. *Terrestrial 1.* <http://140.112.114.62/handle/246246/173899>.
- Clark, M.K., House, M.A., Royden, L.H., Whipple, K.X., Burchfiel, B.C., Zhang, X., Tang, W., 2005. Late cenozoic uplift of southeastern Tibet. *Geology* 33 (6), 525. <https://doi.org/10.1130/G21265.1>.
- Clift, P.D., 2006. Controls on the erosion of Cenozoic Asia and the flux of clastic sediment to the ocean. *Earth Planet Sci. Lett.* 241 (3–4), 571–580. <https://doi.org/10.1016/j.epsl.2005.11.028>.
- Clift, P.D., Sun, Z., 2006. The sedimentary and tectonic evolution of the Yinggehai-Song Hong basin and the southern Hainan margin, South China Sea: implications for Tibetan uplift and monsoon intensification: evolution of yinggehai-song hong basin.

- J. Geophys. Res. Solid Earth 111 (B6). <https://doi.org/10.1029/2005JB004048> n/a-n/a.
- Clift, P.D., Layne, G.D., Blusztajn, J., 2004. The Erosional Record of Tibetan Uplift in the East Asian Marginal Seas. *Continent-Ocean Interactions in the East Asian Marginal Seas*, *Geophys. Monogr.*
- Clift, P.D., Hodges, K.V., Heslop, D., Hannigan, R., Van Long, H., Calves, G., 2008a. Correlation of Himalayan exhumation rates and Asian monsoon intensity. *Nat. Geosci.* 1 (12), 875–880. <https://doi.org/10.1038/ngeo351>.
- Clift, P., Lee, G.H., Anh Duc, N., Barckhausen, U., Van Long, H., Zhen, S., 2008b. Seismic reflection evidence for a Dangerous Grounds miniplate: No extrusion origin for the South China Sea: evidence for a dangerous grounds plate. *Tectonics* 27 (3). <https://doi.org/10.1029/2007TC002216> n/a-n/a.
- Clift, P.D., Wan, S., Blusztajn, J., 2014. Reconstructing chemical weathering, physical erosion and monsoon intensity since 25Ma in the northern South China Sea: a review of competing proxies. *Earth Sci. Rev.* 130, 86–102. <https://doi.org/10.1016/j.earscirev.2014.01.002>.
- Clift, P.D., Brune, S., Quinteros, J., 2015. Climate changes control offshore crustal structure at South China Sea continental margin. *Earth Planet Sci. Lett.* 420, 66–72. <https://doi.org/10.1016/j.epsl.2015.03.032>.
- Clift, P.D., Harff, J., Wu, J., Qiu, Y. (Eds.), 2016. *River-dominated Shelf Sediments of East Asian Seas*. The Geological Society.
- Collins, D.S., Avdis, A., Allison, P.A., Johnson, H.D., Hill, J., Piggott, M.D., Hassan, M.H. A., Damit, A.R., 2017. Tidal dynamics and mangrove carbon sequestration during the oligo-miocene in the south China sea. *Nat. Commun.* 8 (1), 15698 <https://doi.org/10.1038/ncomms15698>.
- Cullen, A., Reemst, P., Henstra, G., Gozzard, S., Ray, A., 2010. Rifting of the south China sea: new perspectives. *Petrol. Geosci.* 16 (3), 273–282. <https://doi.org/10.1144/1354-079309-908>.
- Cung, T.C., Dorobek, S., Richter, C., Flower, M., Kikawa, E., Nguyen, Y.T., McCabe, R., 1998. Paleomagnetism of late Neogene basalts in Vietnam and Thailand: implications for the post-Miocene tectonic history of Indochina. In: Flower, M.F.J., Chung, S., Lo, C., Lee, T. (Eds.), *Geodynamics Series*, vol. 27. American Geophysical Union, pp. 289–299. <https://doi.org/10.1029/GD027p0289>.
- Dadson, S.J., Hovius, N., Chen, H., Dade, W.B., Hsieh, M.-L., Willett, S.D., Hu, J.-C., Horng, M.-J., Chen, M.-C., Stark, C.P., Lague, D., Lin, J.-C., 2003. Links between erosion, runoff variability and seismicity in the Taiwan orogen. *Nature* 426 (6967), 648–651. <https://doi.org/10.1038/nature02150>.
- Ding, Weiwei, Li, Jiaobiao, Han, Xiqiu, Suess, Erwin & Y., Huang, & X., Qui, & M., Li, 2010. Morphotectonics and formation of the Taiwan Bank canyon, southwest offshore taiwan Island. *J. Oceanogr. Mar. Sci.* 14, 65–78.
- Ding, W., Li, J., Li, J., Fang, Y., Tang, Y., 2013. Morphotectonics and evolutionary controls on the Pearl River canyon system, south China sea. *Mar. Geophys. Res.* 34 (3–4), 221–238. <https://doi.org/10.1007/s11001-013-9173-9>.
- Ding, W., Li, J., Clift, P.D., 2016. Spreading dynamics and sedimentary process of the southwest sub-basin, south China sea: constraints from multi-channel seismic data and IODP expedition 349. *J. Asian Earth Sci.* 115, 97–113. <https://doi.org/10.1016/j.jseas.2015.09.013>.
- Ding, W., Sun, Z., Dadd, K., Fang, Y., Li, J., 2018. Structures within the oceanic crust of the central South China Sea basin and their implications for oceanic accretionary processes. *Earth Planet Sci. Lett.* 488, 115–125. <https://doi.org/10.1016/j.epsl.2018.02.011>.
- Ding, W., Sun, Z., Mohn, G., Nirrengarten, M., Tugend, J., Manatschal, G., Li, J., 2020. Lateral evolution of the rift-to-drift transition in the South China Sea: evidence from multi-channel seismic data and IODP Expeditions 367&368 drilling results. *Earth Planet Sci. Lett.* 531, 115932 <https://doi.org/10.1016/j.epsl.2019.115932>.
- Fang, P., Ding, W., Zhao, Y., Lin, X., Zhao, Z., 2022. Detachment-controlled subsidence pattern at hyper-extended passive margin: insights from backstripping modelling of the Baiyun Rift, northern South China Sea. *Gondwana Res.* <https://doi.org/10.1016/j.gr.2021.12.012>. S1342937X22000119.
- Figueiredo, J., Hoorn, C., van der Ven, P., Soares, E., 2009. Late Miocene onset of the Amazon River and the Amazon deep-sea fan: evidence from the foz do amazonas basin. *Geology* 37 (7), 619–622. <https://doi.org/10.1130/G25567A.1>.
- Finlayson, D.P., Montgomery, D.R., Hallet, B., 2002. Spatial coincidence of rapid inferred erosion with young metamorphic massifs in the Himalayas. *Geology* 30 (3), 219. [https://doi.org/10.1130/0091-7613\(2002\)030<0219:SCORIE>2.0.CO;2](https://doi.org/10.1130/0091-7613(2002)030<0219:SCORIE>2.0.CO;2).
- Franke, D., Savva, D., Pubellier, M., Steuer, S., Mouly, B., Auxietre, J.-L., Meresse, F., Chamot-Rooke, N., 2014. The final rifting evolution in the South China Sea. *Mar. Petrol. Geol.* 58, 704–720. <https://doi.org/10.1016/j.marpetgeo.2013.11.020>.
- Fuller, C.W., Willett, S.D., Hovius, N., Slingerland, R., 2003. Erosion rates for taiwan mountain basins: new determinations from suspended sediment records and a stochastic model of their temporal variation. *J. Geol.* 111 (1), 71–87. <https://doi.org/10.1086/344665>.
- Gao, J., Peng, X., Wu, S., Lüdmann, T., McIntosh, K., Ma, B., Xu, Z., 2019. Different expressions of the crustal structure across the Dongsha Rise along the northeastern margin of the South China Sea. *J. Asian Earth Sci.* 171, 187–200. <https://doi.org/10.1016/j.jseas.2018.01.034>.
- Gao, H., Nie, X., Luo, W., 2021. Source to sink" analysis of a sea basin: the Quaternary deepwater turbidite fan system in Pearl River Valley-Northwest subbasin, Northern South China Sea. *Mar. Geol. Quat. Geol.* 41 (2), 1–12. <https://doi.org/10.16562/j.cnki.0256-1492.2020070202> (in Chinese).
- Gong, S.Y., Mii, H.S., Wei, K.Y., Horng, C.S., You, C.F., Huang, F.W., Chi, W.R., Yui, T.F., Torng, P.K., Huang, S.T., Wang, S.W., Wu, J.C., Yang, K.M., 2005. Dry climate near the western pacific warm pool: Pleistocene caliches of the Nansha Islands, south China sea. *Palaeogeogr. Palaeoclimatol. Palaeoecol.* 226 (3–4), 205–213. <https://doi.org/10.1016/j.palaeo.2005.05.012>.
- Gong, C., Wang, Y., Zhu, W., Li, W., Xu, Q., Zhang, J., 2011. The central submarine canyon in the Qiongdongnan Basin, northwestern south China sea: architecture, sequence stratigraphy, and depositional processes. *Mar. Petrol. Geol.* 28 (9), 1690–1702. <https://doi.org/10.1016/j.marpetgeo.2011.06.005>.
- Gong, C., Wang, Y., Zhu, W., Li, W., Xu, Q., 2013. Upper Miocene to quaternary unidirectionally migrating deep-water channels in the Pearl River Mouth basin, northern south China sea. *AAPG (Am. Assoc. Pet. Geol.) Bull.* 97 (2), 285–308. <https://doi.org/10.1306/07121211159>.
- Guan, Y., Yang, S., Song, H., Liu, S., Chen, J., 2016. Study of deep water channels in SW South China Sea based on multi-beam bathymetric and multi-channel reflection seismic data. *Chin. J. Geophys.* 59 (11), 9 (in Chinese).
- Hall, R., 2002. Cenozoic geological and plate tectonic evolution of SE Asia and the SW Pacific: computer-based reconstructions, model and animations. *J. Asian Earth Sci.* 20 (4), 353–431. [https://doi.org/10.1016/S1367-9120\(01\)00069-4](https://doi.org/10.1016/S1367-9120(01)00069-4).
- Hapke, C.J., Lentz, E.E., Gayes, P.T., McCoy, C.A., Hebre, R., Schwab, W.C., Williams, S. J., 2010. A review of sediment budget imbalances along fire Island, New York: can nearshore geologic framework and patterns of shoreline change explain the deficit? *J. Coast Res.* 263, 510–522. <https://doi.org/10.2112/08-1140.1>.
- Haq, B.U., Hardenbol, J., Vail, P.R., 1987. Chronology of fluctuating sea levels since the triassic. *Science* 235 (4793), 1156–1167. <https://doi.org/10.1126/science.235.4793.1156>.
- He, M., Zhong, G., Liu, X., Liu, L., Shen, X., Wu, Z., Huang, K., 2017. Rapid post-rift tectonic subsidence events in the Pearl River Mouth basin, northern south China sea margin. *J. Asian Earth Sci.* 147, 271–283. <https://doi.org/10.1016/j.jseas.2017.07.024>.
- Holbourn, A.E., Kuhnt, W., Clemens, S.C., Kochhann, K.G.D., Jöhnck, J., Lübbbers, J., Andersen, N., 2018. Late Miocene climate cooling and intensification of southeast Asian winter monsoon. *Nat. Commun.* 9 (1), 1584. <https://doi.org/10.1038/s41467-018-03950-1>.
- Honza, E., John, J., Banda, R.M., 2000. An imbrication model for the rajang accretionary complex in sarawak, Borneo. *J. Asian Earth Sci.* 18 (6), 751–759. [https://doi.org/10.1016/S1367-9120\(00\)00044-4](https://doi.org/10.1016/S1367-9120(00)00044-4).
- Huang, W., 2004. Sediment Distributional Patterns and Evolution in the South China Sea since the Oligocene. Tongji University. <https://doi.org/10.7666/d.w1657102> (in Chinese).
- Huang, W., Guan, Y., 2013. The discovery and significance of the deep meander channel in Mekong River. *Geol. Rev.* 59 (z1), 1090 (in Chinese).
- Huang, W., Wang, P., 2006. Sedimentary quantity and distribution of the south China sea since Oligocene. *Sci. China (Ser. D Earth Sciences)* 36 (9), 822–829. <https://doi.org/10.3969/j.issn.1674-7240.2006.09.004> (in Chinese).
- Huang, K., Zhong, G., He, M., Liu, L., Wu, Z., Liu, X., 2018. Growth and linkage of a complex oblique-slip Fault Zone in the Pearl River Mouth basin, northern south China sea. *J. Struct. Geol.* 117, 27–43. <https://doi.org/10.1016/j.jsg.2018.09.002>.
- Huang, X., Betzler, C., Wu, S., Bernhardt, A., Eagles, G., Han, X., Hovland, M., 2020. First documentation of seismic stratigraphy and depositional signatures of Zhongsha atoll (Macacles Bank), South China Sea. *Mar. Petrol. Geol.* 117, 104349 <https://doi.org/10.1016/j.marpetgeo.2020.104349>.
- Huh, C.A., Chen, W., Hsu, F.-H., Su, C.-C., Chiu, J.-K., Lin, S., Liu, C.-S., Huang, B.-J., 2011. Modern (<100 years) sedimentation in the Taiwan Strait: rates and source-to-sink pathways elucidated from radionuclides and particle size distribution. *Continent. Shelf Res.* 31 (1), 47–63. <https://doi.org/10.1016/j.csr.2010.11.002>.
- Jian, Z., Larsen, H.C., Alvarez Zarikian, C.A., 2018. & expedition 368 scientists. In: *International Ocean Discovery Program, vol. 368. Expedition 368 Preliminary Report*.
- Jian, Z., Jin, H., Kaminski, M.A., Ferreira, F., Li, B., Yu, P.-S., 2019. Discovery of the marine Eocene in the northern south China sea. *Natl. Sci. Rev.* 6 (5), 881–885. <https://doi.org/10.1093/nsr/nzw084>.
- Jiang, H., Wan, S., Ma, X., Zhong, N., Zhao, D., 2017. End-member modeling of the grain-size record of Sikouzi fine sediments in Ningxia (China) and implications for temperature control of Neogene evolution of East Asian winter monsoon. *PLoS One* 12 (10), e0186153. <https://doi.org/10.1371/journal.pone.0186153>.
- Jonell, T.N., Clift, P.D., Hoang, L.V., Hoang, T., Carter, A., Wittmann, H., Böning, P., Pahnke, K., Rittenour, T., 2017. Controls on erosion patterns and sediment transport in a monsoonal, tectonically quiescent drainage, Song Gianh, central Vietnam. *Basin Res.* 29, 659–683. <https://doi.org/10.1111/bre.12199>.
- Koppers, A.A., 2014. On the 40 Ar/39 Ar Dating of Low-Potassium Ocean Crust Basalt from IODP Expedition 349, South China Sea. 2014. AGU Fall Meeting Abstracts. T31E-03.
- Kuhlemann, J., Frisch, W., Székely, B., 2002. Post-collisional sediment budget history of the Alps: tectonic versus climatic control. *Int. J. Earth Sci.* 91 (5), 818–837. <https://doi.org/10.1007/s00531-002-0266-y>.
- Kuszniar, N.J., Roberts, A.M., Morley, C.K., 1995. Forward and reverse modelling of rift basin formation. *Geol. Soc., London, Spec. Publ.* 80 (1), 33–56. <https://doi.org/10.1144/GSL.SP.1995.080.01.02>.
- Larsen, H.C., Mohn, G., Nirrengarten, M., Sun, Z., Stock, J., Jian, Z., Klaus, A., Alvarez Zarikian, C.A., Boaga, J., Bowden, S.A., Briais, A., Chen, Y., Cukur, D., Dadd, K., Ding, W., Dorais, M., Ferré, E.C., Ferreira, F., Furusawa, A., et al., 2018. Rapid transition from continental breakup to igneous oceanic crust in the South China Sea. *Nat. Geosci.* 11 (10), 782–789. <https://doi.org/10.1038/s41561-018-0198-1>.
- Lavé, J., Avouac, J.P., 2001. Fluvial incision and tectonic uplift across the Himalayas of central Nepal. *J. Geophys. Res. Solid Earth* 106 (B11), 26561–26591. <https://doi.org/10.1029/2001JB000359>.
- Lavier, L.L., Steckler, M.S., Brigaud, F., 2001. Climatic and tectonic control on the Cenozoic evolution of the West African margin. *Mar. Geol.* 178 (1–4), 63–80. [https://doi.org/10.1016/S0025-3227\(01\)00175-X](https://doi.org/10.1016/S0025-3227(01)00175-X).

- Lei, C., Ren, J., Sternai, P., Fox, M., Willett, S., Xie, X., Clift, P.D., Liao, J., Wang, Z., 2015. Structure and sediment budget of yinggehai-song hong basin, south China sea: implications for cenozoic tectonics and river basin reorganization in Southeast Asia. *Tectonophysics* 655, 177–190. <https://doi.org/10.1016/j.tecto.2015.05.024>.
- Li, C., Song, T., 2012. Magnetic recording of the Cenozoic oceanic crustal accretion and evolution of the South China Sea basin. *Chin. Sci. Bull.* 57 (24), 3165–3181. <https://doi.org/10.1007/s11434-012-5063-9>.
- Li, J., Jin, X., Gao, J., 2002. Rifting characteristics of eastern subbasin of South China Sea and its spreading pattern. *Rifting Characteristics of Eastern Subbasin of South China Sea and Its Spreading Pattern* 21 (1), 77–85.
- Li, J., Ding, W., Gao, J., Wu, Z., Zhang, J., 2011. Cenozoic evolution model of the seafloor spreading in south China sea: new constraints from high resolution geophysical data. *Chin. J. Geophys.* 54 (6), 894–906. <https://doi.org/10.1002/cjg2.1672>.
- Li, J., Ding, W., Wu, Z., Zhang, J., Dong, C., 2012. The propagation of seafloor spreading in the southwestern subbasin, South China Sea. *Chin. Sci. Bull.* 57 (24), 3182–3191. <https://doi.org/10.1007/s11434-012-5329-2>.
- Li, L., Clift, P.D., Nguyen, H.T., 2013. The sedimentary, magmatic and tectonic evolution of the southwestern South China Sea revealed by seismic stratigraphic analysis. *Mar. Geophys. Res.* 34 (3–4), 341–365. <https://doi.org/10.1007/s11001-013-9171-y>.
- Li, C.F., Xu, X., Lin, J., Sun, Z., Zhu, J., Yao, Y., Zhao, X., Liu, Q., Kulhanek, D.K., Wang, J., Song, T., Zhao, J., Qiu, N., Guan, Y., Zhou, Z., Williams, T., Bao, R., Briais, A., Brown, E.A., et al., 2014. Ages and magnetic structures of the South China Sea constrained by deep tow magnetic surveys and IODP Expedition 349. *G-cubed* 15 (12), 4958–4983. <https://doi.org/10.1002/2014GC005567>.
- Li, C.F., Li, J., Ding, W., Franke, D., Yao, Y., Shi, H., Pang, X., Cao, Y., Lin, J., Kulhanek, D.K., Williams, T., Bao, R., Briais, A., Brown, E.A., Chen, Y., Clift, P.D., Colwell, F.S., Dadd, K.A., Hernández-Almeida, I., et al., 2015a. Seismic stratigraphy of the central South China Sea basin and implications for neotectonics. *J. Geophys. Res. Solid Earth* 120 (3), 1377–1399. <https://doi.org/10.1002/2014JB011686>.
- Li, C.F., Lin, J., Kulhanek, D.K., 2015b. And the expedition 349 scientists. In: Proceedings of the International Ocean Discovery Program, vol. 349. *South China Sea Tectonics: College Station, TX (International Ocean Discovery Program)*. <http://publications.iodp.org/proceedings/349/349title.html>.
- Liu, D., Zheng, M., Guo, Z., 1998. The initiation and evolution of the Asian monsoon system timely coupled with the ice sheet growth and the tectonic movements in Asia. *J. Quat. Sci.* 18 (3), 194–204 (in Chinese).
- Liu, Z., Colin, C., Huang, W., Le, K.P., Tong, S., Chen, Z., Trentesaux, A., 2007. Climatic and tectonic controls on weathering in south China and Indochina Peninsula: clay mineralogical and geochemical investigations from the Pearl, Red, and Mekong drainage basins: controls on weathering in S. China. *G-cubed* 8 (5). <https://doi.org/10.1029/2006GC001490> n/a-n/a.
- Liu, J.P., Liu, C.S., Xu, K.H., Milliman, J.D., Chiu, J.K., Kao, S.J., Lin, S.W., 2008. Flux and fate of small mountainous rivers derived sediments into the Taiwan Strait. *Mar. Geol.* 256 (1–4), 65–76. <https://doi.org/10.1016/j.margeo.2008.09.007>.
- Liu, Z., Zhao, Y., Colin, C., Stattegger, K., Wiesner, M.G., Hu, C.-A., Zhang, Y., Li, X., Sompongchaiyakul, P., You, C.-F., Huang, C.-Y., Liu, J.T., Siriring, F.P., Le, K.P., Sathiamurthy, E., Hantoro, W.S., Liu, J., Tuo, S., Zhao, S., et al., 2016. Source-to-sink transport processes of fluvial sediments in the South China Sea. *Earth Sci. Rev.* 153, 238–273. <https://doi.org/10.1016/j.earscirev.2015.08.005>.
- Liu, C., Clift, P.D., Carter, A., Böning, P., Hu, Z., Sun, Z., Pahnke, K., 2017a. Controls on modern erosion and the development of the Pearl River drainage in the late Paleogene. *Mar. Geol.* 394, 52–68. <https://doi.org/10.1016/j.margeo.2017.07.011>.
- Liu, C., Clift, P.D., Murray, R.W., Blusztajn, J., Ireland, T., Wan, S., Ding, W., 2017b. Geochemical evidence for initiation of the modern Mekong delta in the southwestern South China Sea after 8 Ma. *Chem. Geol.* 451, 38–54. <https://doi.org/10.1016/j.chemgeo.2017.01.008>.
- Liu, C., Hou, W., Qiu, Z., et al., 2019. Sedimentary evolution and controls in paleo-Hanjiang delta from 32 to 10.5 Ma[J]. *PETROLEUM GEOLOGY & EXPERIMENT* 41 (4), 482–490 (In Chinese with English abstract).
- Liu, H., Yumul, G.P., Dimalanta, C.B., Queano, K., Xia, X., Peng, T., Lan, J., Xu, Y., Yan, Y., Guotana, J.M.R., Olindo, V.S., 2020. Western northern Luzon isotopic evidence of transition from proto-south China sea to south China sea fossil ridge subduction. *Tectonics* 39 (2). <https://doi.org/10.1029/2019TC005639>.
- Liu, X., Chen, X., Sun, K., Li, C., 2021. Provenance of U1431 sediments from the eastern subbasin of the south China sea since middle Miocene. *Earth Sci.* 46 (3), 1008–1022 (in Chinese).
- Liu, C., Stockli, D.F., Clift, P.D., Wan, S., Stockli, L.D., Höfig, T.W., Schindlbeck-Belo, J. C., 2022. Geochronological and geochemical characterization of paleo-rivers deposits during rifting of the South China Sea. *Earth Planet Sci. Lett.* 584, 117427.
- Luan, X., Zhang, L., Peng, X., 2012. Dongsha erosive channel on northern south China sea shelf and its induced kuroshio south China sea branch. *Sci. China Earth Sci.* 55 (1), 149–158. <https://doi.org/10.1007/s11430-011-4322-y>.
- Lüdmann, T., Wong, H.K., 1999. Neotectonic regime on the passive continental margin of the northern South China Sea. *Tectonophysics* 311 (1–4), 113–138. [https://doi.org/10.1016/S0040-1951\(99\)00155-9](https://doi.org/10.1016/S0040-1951(99)00155-9).
- Lüdmann, T., Kin Wong, H., Wang, P., 2001. Plio–Quaternary sedimentation processes and neotectonics of the northern continental margin of the South China Sea. *Mar. Geol.* 172 (3–4), 331–358. [https://doi.org/10.1016/S0025-3227\(00\)00129-8](https://doi.org/10.1016/S0025-3227(00)00129-8).
- Luo, W., Zhou, J., Li, X., Yao, Y., Wang, Z., 2018. Morphology and structure and evolution of west basin canyon, south China sea. *Earth Sci.* 43 (6), 2172–2183 (in Chinese).
- Ma, X., Tian, J., 2015. East Asian monsoon evolution and aridification of Northwest China viewed from land and sea on the tectonic-orbital time scale since 15Ma. *Quat. Sci.* 35 (6), 1320–1330. <https://doi.org/10.11928/j.issn.1001-7410.2015.06.02> (in Chinese).
- Ma, Y., Wu, S., Lv, F., Dong, D., Sun, Q., Lu, Y., Gu, M., 2011. Seismic characteristics and development of the Xisha carbonate platforms, northern margin of the South China Sea. *J. Asian Earth Sci.* 40 (3), 770–783. <https://doi.org/10.1016/j.jseas.2010.11.003>.
- Ma, M., Li, C., Lv, C., Chen, G., Yang, F., Yan, Y., et al., 2017. Geochemistry and provenance of a multiple-stage fan in the upper Miocene to the Pliocene in the Yinggehai and qiongdongnan basins, offshore south China sea. *Mar. Petrol. Geol.* 79, 64–80.
- Ma, M., Chen, G., Lyu, C., et al., 2019. The formation and evolution of the paleo-Pearl River and its influence on the source of the northern South China sea[J]. *Mar. Petrol. Geol.* 106, 171–189.
- Miao, Y., Warny, S., Clift, P.D., Liu, C., Gregory, M., 2017. Evidence of continuous Asian summer monsoon weakening as a response to global cooling over the last 8 Ma. *Gondwana Res.* 52, 48–58. <https://doi.org/10.1016/j.gr.2017.09.003>.
- Milliman, J.D., Farnsworth, K.L., 2011. River Discharge to the Coastal Ocean: A Global Synthesis. Cambridge University Press. <https://doi.org/10.1017/CBO9780511781247>.
- Milliman, J.D., Syvitski, J.P.M., 1992. Geomorphic/tectonic control of sediment discharge to the ocean: the importance of small mountainous rivers. *J. Geol.* 100 (5), 525–544. <https://doi.org/10.1086/629606>.
- Murray, M.R., Dorobek, S.L., 2004. Sediment supply, tectonic subsidence, and basin-filling patterns across the southwestern South China Sea during Pliocene to recent time. In: Clift, P., Kuhnt, W., Wang, P., Hayes, D. (Eds.), *Geophysical Monograph Series*, vol. 149. American Geophysical Union, pp. 235–254. <https://doi.org/10.1029/149GM13>.
- Nirrengarten, M., Mohn, G., Kusznir, N.J., Sapin, F., Despinois, F., Pubellier, M., Chang, S.P., Larsen, H.C., Ringenbach, J.C., 2020. Extension modes and breakup processes of the southeast China-Northwest Palawan conjugate rifted margins. *Mar. Petrol. Geol.* 113, 104123. <https://doi.org/10.1016/j.marpetgeo.2019.104123>.
- Pang, X., Chen, C.M., Shi, H.S., Shu, Y., Shao, L., He, M., Shen, J., 2005. Response between relative sea-level change and the Pearl River deep-water fan system in the South China Sea. *Earth Sci. Front.* 12, 167–177 (in Chinese).
- Pautot, G., Rangin, C., Briais, A., Wu, J., Han, S., Li, H., Lu, Y., Zhao, J., 1990. The axial ridge of the south China sea-a-seabean and geophysical survey. *Oceanol. Acta* 13 (2), 129–143.
- Peng, D., Pang, X., Chen, C., Zhu, M., Huang, X., Shu, Y., 2006. The characteristics and controlling factors for the formation of deep-water fan system in south China sea. *Acta Sedimentol. Sin.* 24 (1), 10–18. <https://doi.org/10.3969/j.issn.1000-0550.2006.01.002> (in Chinese).
- Prell, W.L., Wang, P., Blum, P., Rea, D.K., Clemens, S.C. (Eds.), 2006. *Proceedings of the Ocean Drilling Program, 184 Scientific Results*, vol. 185. Ocean Drilling Program. <https://doi.org/10.2973/odp.proc.sr.184.2006>.
- Rangin, C., Bellon, H., Benard, F., Letouzey, J., Muller, C., Sanudin, T., 1990. Neogene arc-continent collision in sabah, northern Borneo (Malaysia). *Tectonophysics* 183 (1–4), 305–319. [https://doi.org/10.1016/0040-1951\(90\)90423-6](https://doi.org/10.1016/0040-1951(90)90423-6).
- Savva, D., Pubellier, M., Franke, D., Chamot-Rooke, N., Meresse, F., Steuer, S., Auxietre, J.L., 2014. Different expressions of rifting on the South China Sea margins. *Mar. Petrol. Geol.* 58, 579–598. <https://doi.org/10.1016/j.marpetgeo.2014.05.023>.
- Schimanski, A., 2002. Holocene Sedimentation on the Vietnamese Shelf: from Source to Sink. https://macau.uni-kiel.de/receive/diss_mods_00000610.
- Shang, Z., Xie, X., Li, X., Zhang, D., He, Y., Yang, X., Cui, M., 2015. Difference in full-filled time and its controlling factors in the central canyon of the Qiongdongnan Basin. *Acta Oceanol. Sin.* 34 (10), 81–89. <https://doi.org/10.1007/s13131-015-0717-5>.
- Shao, L., Liu, Y., Pang, X., Wei, G., Li, X., Jian, Z., Wang, P., 2004. Sedimentary record of the tectonic evolution of the South China Sea since the Oligocene: evidence from deep sea sediments of ODP Site 1148. *Adv. Earth Sci.* 19 (4), 539–544. <https://doi.org/10.3321/j.issn:1001-8166.2004.04.008> (in Chinese).
- Shao, L., Cao, L., Pang, X., et al., 2016. Detrital zircon provenance of the Paleogene syn-rift sediments in the northern South China Sea[J]. *G-cubed* 17 (2), 255–269.
- Shao, L., Li, Q., Zhu, W., Zhang, D., Qiao, P., Liu, X., You, L., Cui, Y., Dong, X., 2017. Neogene carbonate platform development in the NW South China Sea: litho-, bio- and chemo-stratigraphic evidence. *Mar. Geol.* 385, 233–243. <https://doi.org/10.1016/j.margeo.2017.01.009>.
- Shao, L., Cui, Y., Stattegger, K., Zhu, W., Qiao, P., Zhao, Z., 2019. Drainage control of Eocene to Miocene sedimentary records in the southeastern margin of Eurasian Plate. *GSA Bulletin* 131 (3–4), 461–478. <https://doi.org/10.1130/B32053.1>.
- Shi, X., Kohn, B., Spencer, S., Guo, X., Li, Y., Yang, X., Shi, H., Gleadow, A., 2011. Cenozoic denudation history of southern Hainan Island, South China Sea: constraints from low temperature thermochronology. *Tectonophysics* 504 (1–4), 100–115. <https://doi.org/10.1016/j.tecto.2011.03.007>.
- Sibuet, J.-C., Hsu, S.-K., 2004. How was Taiwan created? *Tectonophysics* 379 (1–4), 159–181. <https://doi.org/10.1016/j.tecto.2003.10.022>.
- Sibuet, J.-C., Yeh, Y.-C., Lee, C.-S., 2016. Geodynamics of the south China sea. *Tectonophysics* 692, 98–119. <https://doi.org/10.1016/j.tecto.2016.02.022>.
- Steuer, S., Franke, D., Meresse, F., Savva, D., Pubellier, M., Auxietre, J.-L., 2014. Oligocene–Miocene carbonates and their role for constraining the rifting and collision history of the Dangerous Grounds, South China Sea. *Mar. Petrol. Geol.* 58, 644–657. <https://doi.org/10.1016/j.marpetgeo.2013.12.010>.
- Su, M., Zhang, C., Xie, X., Wang, Z., Jiang, T., He, Y., Zhang, C., 2014. Controlling factors on the submarine canyon system: a case study of the central canyon system in the Qiongdongnan Basin, northern south China sea. *Sci. China Earth Sci.* 57 (10), 2457–2468. <https://doi.org/10.1007/s11430-014-4878-4>.
- Su, M., Xie, X., Wang, Z., Jiang, T., Zhang, C., He, Y., 2016. Sedimentary evolution of the central canyon system in the Qiongdongnan Basin, northern south China sea. *Petrol. Res.* 1 (1), 81–92. [https://doi.org/10.1016/S2096-2495\(17\)30033-9](https://doi.org/10.1016/S2096-2495(17)30033-9).

- Sun, X., Wang, P., 2005. How old is the Asian monsoon system?—palaeobotanical records from China. *Palaeogeogr. Palaeoclimatol. Palaeoecol.* 222 (3–4), 181–222. <https://doi.org/10.1016/j.palaeo.2005.03.005>.
- Sun, Q., Wu, S., Cartwright, J., Wang, S., Lu, Y., Chen, D., Dong, D., 2014. Neogene igneous intrusions in the northern South China Sea: evidence from high-resolution three dimensional seismic data. *Mar. Petrol. Geol.* 54, 83–95. <https://doi.org/10.1016/j.marpetgeo.2014.02.014>.
- Sun, B., Wang, Y.-F., Li, C.-S., Yang, J., Li, J.-F., Li, Y.-L., Deng, T., Wang, S.-Q., Zhao, M., Spicer, R.A., Ferguson, D.K., Mehrotra, R.C., 2015. Early Miocene elevation in northern Tibet estimated by palaeobotanical evidence. *Sci. Rep.* 5 (1), 10379. <https://doi.org/10.1038/srep10379>.
- Sun, Z., Jian, Z., Stock, J.M., Larsen, H.C., Klaus, A., Alvarez Zarikian, C.A., 2018. Volume 367/368. In: South China Sea Rifted Margin (Expedition 367/368 Scientists, 367/378. International Ocean Discovery Program. <https://doi.org/10.14379/iodp.proc.367368.org.2018>.
- Sun, Z., Ding, W., Zhao, X., Qiu, N., Lin, J., Li, C., 2019. The latest spreading periods of the south China sea: new constraints from macrostructure analysis of IODP expedition 349 cores and geophysical data. *J. Geophys. Res. Solid Earth* 124 (10), 9980–9998. <https://doi.org/10.1029/2019JB017584>.
- Taylor, B., Hayes, D.E., 1980. The tectonic evolution of the South China Basin. In: Hayes, D.E. (Ed.), *Geophysical Monograph Series*, vol. 23. American Geophysical Union, pp. 89–104. <https://doi.org/10.1029/GM023p0089>.
- Taylor, B., Hayes, D.E., 1983. Origin and history of the south China sea basin. In: Hayes, D.E. (Ed.), *Geophysical Monograph Series*, vol. 27. American Geophysical Union, pp. 23–56. <https://doi.org/10.1029/GM027p0023>.
- Wan, S., Li, A., Clift, P.D., Jiang, H., 2006. Development of the east asian summer monsoon: evidence from the sediment record in the south China sea since 8.5 Ma. *Palaeogeogr. Palaeoclimatol. Palaeoecol.* 241 (1), 139–159. <https://doi.org/10.1016/j.palaeo.2006.06.013>.
- Wan, S., Li, A., Clift, P.D., Stuit, J.-B.W., 2007. Development of the east asian monsoon: mineralogical and sedimentologic records in the northern south China sea since 20 Ma. *Palaeogeogr. Palaeoclimatol. Palaeoecol.* 254 (3–4), 561–582. <https://doi.org/10.1016/j.palaeo.2007.09.009>.
- Wan, S., Li, A., Clift, P.D., Wu, S., Xu, K., Li, T., 2010. Increased contribution of terrigenous supply from Taiwan to the northern South China Sea since 3Ma. *Mar. Geol.* 278 (1–4), 115–121. <https://doi.org/10.1016/j.margeo.2010.09.008>.
- Wang, P., Li, Q. (Eds.), 2009. *The South China Sea: Paleoceanography and Sedimentology*. Springer.
- Wang, P., Zhao, Q., Jian, Z., Cheng, X., Huang, W., Tian, J., Wang, J., Li, Q., Li, B., Su, X., 2003. Thirty million year deep sea records in the South China Sea. *Chin. Sci. Bull.* 48 (23), 2524–2535. <https://doi.org/10.1007/BF03037016>.
- Wang, E., Kirby, E., Furlong, K.P., van Soest, M., Xu, G., Shi, X., Kamp, P.J.J., Hodges, K. V., 2012. Two-phase growth of high topography in eastern Tibet during the Cenozoic. *Nat. Geosci.* 5 (9), 640–645. <https://doi.org/10.1038/geo1538>.
- Wang, X., Wang, Y., He, M., Chen, W., Zhuo, H., Gao, S., Wang, M., Zhou, J., 2017. Genesis and evolution of the mass transport deposits in the middle segment of the Pearl River canyon, South China Sea: insights from 3D seismic data. *Mar. Petrol. Geol.* 88, 555–574. <https://doi.org/10.1016/j.marpetgeo.2017.08.036>.
- Wang, P., Huang, C.-Y., Lin, J., Jian, Z., Sun, Z., Zhao, M., 2019. The South China Sea is not a mini-Atlantic: plate-edge rifting vs intra-plate rifting. *Natl. Sci. Rev.* 6 (5), 902–913. <https://doi.org/10.1093/nsr/nwz135>.
- Wang, W., Yang, X., Bidgoli, T.S., et al., 2019. Detrital zircon geochronology reveals source-to-sink relationships in the Pearl River Mouth Basin, China[J]. *Sediment. Geol.* 388, 81–98.
- Wang, F., Wu, Y., Ding, W., 2021. Sedimentary budget and controlling factors of the northwest and southwest sub-basins, the south China sea. *Earth Sci.* 46 (3), 986–1007 (in Chinese).
- Wang, W., Zhang, P., Garzione, C.N., Liu, C., Zhang, Z., Pang, J., Wang, Y., Zheng, D., Zheng, W., Zhang, H., 2022. Pulsed rise and growth of the Tibetan Plateau to its northern margin since ca. 30 Ma. *Proc. Natl. Acad. Sci. USA* 119 (8), e2120364119. <https://doi.org/10.1073/pnas.2120364119>.
- Webster, P.J., Magaña, V.O., Palmer, T.N., Shukla, J., Tomas, R.A., Yanai, M., Yasunari, T., 1998. Monsoons: processes, predictability, and the prospects for prediction. *J. Geophys. Res.: Oceans* 103 (C7), 14451–14510. <https://doi.org/10.1029/97JC02719>.
- Wei, G., Liu, Y., Ma, J., Xie, L., Chen, J., Deng, W., Tang, S., 2012. Nd, Sr isotopes and elemental geochemistry of surface sediments from the South China Sea: implications for Provenance Tracing. *Mar. Geol.* 319 (322), 21–34. <https://doi.org/10.1016/j.margeo.2012.05.007>.
- Wu, S., Qin, Z., Wang, D., Peng, X., Wang, Z., Yao, G., 2011. Seismic characteristics and triggering mechanism analysis of mass transport deposits in the northern continental slope of the South China Sea. *Chin. J. Geophys.* 54 (12), 3184–3195. <https://doi.org/10.3969/j.issn.0001-5733.2011.12.018> (in Chinese).
- Wu, S., Yang, Z., Wang, D., Lü, F., Lüdemann, T., Fulthorpe, C., Wang, B., 2014. Architecture, development and geological control of the Xisha carbonate platforms, northwestern South China Sea. *Mar. Geol.* 350, 71–83. <https://doi.org/10.1016/j.margeo.2013.12.016>.
- Wu, Y., Ding, W., Sun, Z., Dong, C., Fang, Y., 2018. Sedimentary budget of the southwest sub-basin, south China sea: controlling factors and geological implications. *Geol. J.* 53 (6), 3082–3092. <https://doi.org/10.1002/gj.3145>.
- Wu, Y., Ding, W., Clift, P.D., Li, J., Yin, S., Fang, Y., Ding, H., 2019. Sedimentary budget of the northwest sub-basin, south China sea: controlling factors and geological implications. *Int. Geol. Rev.* 62 (7–8), 970–987. <https://doi.org/10.1080/00206814.2019.1597392>.
- Xie, X., Müller, R.D., Li, S., Gong, Z., Steinberger, B., 2006. Origin of anomalous subsidence along the Northern South China Sea margin and its relationship to dynamic topography. *Mar. Petrol. Geol.* 23 (7), 745–765. <https://doi.org/10.1016/j.marpetgeo.2006.03.004>.
- Xie, H., Zhou, D., Pang, X., Li, Y., Wu, X., Qiu, N., Li, P., Chen, G., 2013. Cenozoic sedimentary evolution of deepwater sags in the Pearl River Mouth basin, northern south China sea. *Mar. Geophys. Res.* 34 (3–4), 159–173. <https://doi.org/10.1007/s11001-013-9183-7>.
- Xie, X., Ren, J., Pang, X., Lei, C., Chen, H., 2019. Stratigraphic architectures and associated unconformities of Pearl River Mouth basin during rifting and lithospheric breakup of the South China Sea. *Mar. Geophys. Res.* 40 (2), 129–144. <https://doi.org/10.1007/s11001-019-09378-6>.
- Xie, X., Zhu, W., Li, X., Yao, Y., Jiang, T., Liang, C., 2020. Deposition in the south China sea deep basin. *Sci. Technol. Rev.* 38 (18), 62–67 (in Chinese).
- Xie, H., Zhou, D., Shi, H., Kong, D., Li, Y., Li, F., Cao, J., 2021. Lithospheric stretching-style variations and anomalous post-rift subsidence in the deep water sub-basins of the Pearl River Mouth Basin, northern South China Sea. *Mar. Petrol. Geol.* 131, 105140. <https://doi.org/10.1016/j.marpetgeo.2021.105140>.
- Yan, Q., Shi, X., Wang, K., Bu, W., Xiao, L., 2008. Major element, trace element, and Sr, Nd and Pb isotope studies of Cenozoic basalts from the South China Sea. *Sci. China Earth Sci.* 51 (4), 550–566. <https://doi.org/10.1007/s11430-008-0026-3>.
- Yan, Y., Carter, A., Palk, C., Brichau, S., Hu, X., 2011. Understanding sedimentation in the Song hong-Yinggehai basin, south China sea: sedimentation in the Yinggehai Basin. *G-cubed* 12 (6). <https://doi.org/10.1029/2011GC003533> n/a-n/a.
- Yang, S., 2006. Advances in sedimentary geochemistry and tracing applications of asian rivers. *Adv. Earth Sci.* 21 (6), 648–655. <https://doi.org/10.11867/j.issn.1001-8166.2006.06.06>.
- Yao, G., Yuan, S., Wu, S., Zhong, C., 2008. Double provenance depositional model and exploration prospect in the deep-water area of Qiongdongnan Basin. *Petrol. Explor. Dev.* 35 (6), 685–691. [https://doi.org/10.1016/S1876-3804\(09\)60101-4](https://doi.org/10.1016/S1876-3804(09)60101-4).
- Yin, S., Wang, L., Guo, Y., Zhong, G., 2015. Morphology, sedimentary characteristics, and origin of the Dongsha submarine canyon in the northeastern continental slope of the South China Sea. *Sci. China Earth Sci.* 58 (6), 971–985. <https://doi.org/10.1007/s11430-014-5044-8>.
- Yin, S., Li, J., Ding, W., Sawyer, D.E., Wu, Z., Tang, Y., 2018. Sedimentary filling characteristics of the South China Sea oceanic basin, with links to tectonic activity during and after seafloor spreading. *Int. Geol. Rev.* 62 (7–8), 887–907. <https://doi.org/10.1080/00206814.2018.1522603>.
- Yin, S., Li, J., Ding, W., Gao, J., Ding, W., Wang, Y., 2020. Migration of the lower North Palawan submarine canyon: characteristics and controls. *Int. Geol. Rev.* 62 (7–8), 988–1005. <https://doi.org/10.1080/00206814.2018.1522519>.
- Yu, X., Li, S., Qiao, Y., Gao, Y., 2016. The Cenozoic changes of seas and lands and sedimentary filling responses of different basins in northern South China Sea. *J. Palaeogeogr.* 18 (3), 349–366. <https://doi.org/10.7605/gdixb.2016.03.025.6> (in Chinese).
- Zachos, J., Pagani, M., Sloan, L., Thomas, E., Billups, K., 2001. Trends, rhythms, and aberrations in global climate 65 Ma to present. *Science* 292 (5517), 686–693. <https://doi.org/10.1126/science.1059412>.
- Zhang, P., Molnar, P., Downs, W.R., 2001. Increased sedimentation rates and grain sizes 2–4 Myr ago due to the influence of climate change on erosion rates. *Nature* 410 (6831), 891–897. <https://doi.org/10.1038/35073504>.
- Zhang, X., Chen, L., She, Q., Zhang, S., Qiao, P., Shao, L., 2012. Provenance evolution of the paleo-hanjiang River in the northern south China sea, 2012 Mar. *Geol. Quat. Geol.* 32 (4), 41–48. <https://doi.org/10.3724/SP.J.1140.2012.04041> (in Chinese).
- Zhao, Z., Sun, Z., Wang, Z., Sun, Z., Liu, J., Zhang, C., 2015. The high resolution sedimentary filling in Qiongdongnan Basin, northern south China sea. *Mar. Geol.* 361, 11–24. <https://doi.org/10.1016/j.margeo.2015.01.002>.
- Zhao, R., Chen, S., Olariu, C., Steel, R., Zhang, J., Wang, H., 2019. A model for oblique accretion on the south China sea margin; Red River (Song hong) sediment transport into Qiongdongnan Basin since upper Miocene. *Mar. Geol.* 416, 106001. <https://doi.org/10.1016/j.margeo.2019.106001>.
- Zhao, Y., Ding, W., Yin, S., Li, J., Zhang, J., Ding, H., 2020. Asymmetric post-spreading magmatism in the South China Sea: based on the quantification of the volume and its spatiotemporal distribution of the seamounts. *Int. Geol. Rev.* 62 (7–8), 955–969. <https://doi.org/10.1080/00206814.2019.1577189>.
- Zhu, W., Zhang, G., Gao, L., 2008. Geological characteristics and exploration objectives of hydrocarbons in the northern continental margin basin of South China Sea. *Acta Pet. Sin.* 29 (1), 1–9. <https://doi.org/10.3321/j.issn:0253-2697.2008.01.001> (in Chinese).
- Zhu, S., Yao, Y., Luo, W., Xu, Z., Ju, D., Liu, S., 2017. Geomorphologic unit partition, characteristics and genesis of central and western south China sea. *Acta Geosci. Sin.* 38 (6), 897–909. <https://doi.org/10.3975/cagbs.2017.06.05> (in Chinese).